

Adsorption model for atoms and molecules on doped semiconducting oxidesAbhinav S. Raman , Colin Lehman-Chong, and Aleksandra Vojvodic ^{*}*Department of Chemical and Biomolecular Engineering, University of Pennsylvania, Philadelphia, Pennsylvania 19104, USA*

(Received 11 July 2023; revised 14 February 2024; accepted 26 March 2024; published 6 May 2024)

Fundamental understanding of the interaction between atoms and molecules with the surfaces of oxides including semiconducting oxides is crucial for the development of several thermo-, photo-, and electrocatalytic reactions as well as any application where surfaces are exposed to an environment beyond vacuum. While previous studies have postulated material features (descriptors) that to some extent suggest the adsorption energy trends on semiconducting oxides, a physics based model to describe the interaction of atoms and molecules with the surfaces of these materials is still lacking. In this study, we perform a series of controlled *in silico* experiments involving doping of quintessential semiconducting oxides (SrTiO₃, SrZrO₃, and TiO₂) to identify the perturbation by the dopant to the electronic structure of the host oxide and its resultant effect on the adsorption energies of simple atoms and molecules. We identify that a combination of three surface features: unique surface resonance states of the host-metal and lattice oxygen atoms of the terminating surface oxide layer as well as the gap states dominated by the introduced dopants contribute to the adsorption energy in a concerted fashion. We find that this intricate interplay between on the one hand host-metal and on the other hand oxygen surface resonance states with the adsorbate, respectively, results in a deviation from the well-established adsorbate scaling relations seen for NH_x ($x = 0-2$) and CH_x ($x = 0-3$) but not OH_x and SH_x. Through this lens, we develop a physics based adsorption model hitherto referred as the generalized concerted coupling model (GCC model). The introduced model provides a physical understanding with an associated electronic structure descriptor rooted in the unique surface resonances that accurately captures the adsorption energy trends on doped semiconducting oxides. This paves the way for the atomistic design of doped semiconducting oxides for different catalytic applications, including sustainable energy applications such as electrochemical water splitting.

DOI: [10.1103/PhysRevB.109.195416](https://doi.org/10.1103/PhysRevB.109.195416)**I. INTRODUCTION**

Owing to desirable properties such as their high stability, and large relative earth-abundance, semiconducting oxides such as TiO₂ and SrTiO₃ are ubiquitously encountered in several applications ranging from water treatment and air purification to photocatalysis [1,2]. At the crux of all of these applications is the formation of a chemical bond between the oxide surface and interacting atoms or molecules. Therefore resolving scientific problems and optimizing the performance of these semiconducting oxides requires a fundamental description of the chemisorption process, which has been an active area of research over the past several years using both experimental and computational approaches [2–7]. Material features, especially those based on the electronic structure are the most sought after in recent times, with several [8–18] found to provide reasonable correlation with the adsorption energies of certain atoms and molecules on oxide surfaces. This approach has only gained further popularity with the advent of data science and machine learning (ML) approaches in the physical and chemical sciences [19–21]. Among these, the oxygen O-2*p* band center [10] has emerged as a simple descriptor that provides a suitable correlation with the adsorption energies of typical reaction intermediates involved

in the oxygen evolution/reduction reactions. However, the bulk O-2*p* band center cannot capture the changes to the surface electronic structure, especially involving surface or near-surface doping, as well as surface defects that are inherent to surface-mediated processes involving semiconducting oxides.

While there are several other “correlation”-based descriptors that have also been proposed, to the best of our knowledge, there has been very little effort in the development of a physics-based adsorption model and addressing link and origin of the descriptors. For example, the work of Bagus and Illas [22], which presents a novel approach to decompose the different contributions to the chemisorption of atoms and molecules, has been used to understand the interaction of several adsorbates using simple cluster models as well as extended surfaces of metal oxides such as MgO, TiO₂, and complex oxides such as La₂CuO₄ to name a few [23–28]. However, going beyond just decomposition analysis to the identification of a surface electronic structure descriptor that is rooted in physics, akin to what the *d*-band model [29] accomplishes for the adsorption of atoms and molecules on transition metal surfaces, is still lacking. The development of such a model would help unravel the important surface electronic structure features that contribute to the surface reactivity of oxide surfaces, providing a path toward the rational design of these materials for their myriad applications. Herein, we develop such a model for a class of oxides; specifically idealized

^{*}alevoj@seas.upenn.edu

doped oxides with a well-defined heterostructure formed by substitutionally doping the subsurface of semiconducting host oxides with $3d$, $4d$, and $5d$ transition metals. We wish to note here that doping can involve everything from dispersed “heteroatoms” forming solid solutions to the precise substitution of a monolayer of atoms. Indeed, this has given rise to a very broad nomenclature ranging from heterostructured oxides and oxide superlattices to δ doped oxides [30] to describe similar systems such as the ones considered in this study. However, we would like to refer to these systems as “idealized” doped semiconducting oxides owing to them serving as the “ideal” template for the construction of the proposed model.

Doped heterostructured oxides with a semiconducting host have been shown to activate an otherwise inert host in electrochemical water splitting without light illumination. In our previous study, we have identified a generalized tuning mechanism by analyzing the adsorption trends of the different intermediates using first-principles density functional theory (DFT) [31,32]. Systematic introduction of dopants to a semiconducting host oxide was found to induce a perturbation to its electronic structure. The causative effect of this perturbation on the resultant adsorption energy serves as an ideal template to explore the physical origins of the interaction of atoms and molecules with the oxide surface. Indeed, this was the motivation for considering the specific doping strategy employed in this study. This approach also lends itself towards deciphering the origin of the adsorbate scaling relations on oxides [33,34], one crucial piece in the design of these materials for catalytic applications. We therefore first considered the adsorption of OH_x ($x = 0-1$), NH_x ($x = 0-2$), CH_x ($x = 0-3$), SH_x ($x = 0-1$), and H on well-defined surfaces of both subsurface doped perovskite [SrTiO_3 (STO) and SrZrO_3 (SZO)] and rutile oxides (TiO_2), using DFT, and established adsorbate scaling relations. We emphasize here that the particular choice of adsorbates stems from the seminal work of Frank Abild-Pedersen *et al.* [35] on the adsorbate scaling relations of transition metals. Since our primary motivation is the development of a physics-based model that can provide a similar understanding of the adsorbate scaling relations on idealized doped semiconducting oxides, we focus exclusively on these adsorbates. We note that molecules that may physisorb, including NH_3 , CH_4 , etc. are not considered in this study and may indeed require further refinements of the developed model, which exclusively deals with chemisorption. Following this, we performed a series of *in silico* experiments coupled with a detailed analysis of the electronic structure to establish the causal link between the changes to the electronic structure and the adsorption energy. Using this approach, we identified an electronic structure descriptor and established an adsorption model, hitherto referred as the generalized concerted coupling model (GCC model) to describe the interactions between atoms and molecules with doped semiconducting oxides. Using the GCC model, we are able to explain the scaling relations and deviation from their typical expressions as well as understand the adsorption site preference for different adsorbates.

We note, however, that more complex doped semiconducting oxides involving well-dispersed heteroatoms that form solid solutions, including dopants acting as the active sites on the surface are all possible, but are beyond the scope of

this current study and will be considered in future efforts. In addition, surface defects, especially oxygen vacancies formed under reaction conditions, are inherent to the surface chemistry of reducible oxides [2] and will also be accounted for in future refinements of the model. Although the exact formulation of the model may change in order to account for these different effects; the basic concepts introduced in this study provide a completely “generalized” description of the adsorption of atoms and molecules on oxide surfaces. Importantly, the experimental realization of the highly idealized doped semiconducting oxides considered in this study has indeed been achieved and has shown tremendous promise in electrochemical water splitting [31]. Therefore the development of the present model is relevant both to current practical applications involving these oxides while also providing an appropriate platform for describing more complex systems.

II. RESULTS AND DISCUSSION

A. Adsorption of atoms and molecules: trends and scaling relations

We first calculated the adsorption energies of simple atoms and molecules on specific surfaces of subsurface doped semiconducting oxides. Specifically, we considered the (001)- BO_2 surface of the perovskite oxides STO and SZO, as well as the (110) surface of the rutile oxide TiO_2 . We will use the STO as the prototypical host oxide and exemplify our findings, analysis, and model for this system (data on other systems can be found in Ref. [36]). We also note that while the absolute magnitude of the adsorption energy would critically depend on the choice of the reference state of the adsorbate, it is not the aim of this study or the proposed model to reproduce the absolute magnitudes. Instead, the focus is principally on understanding the relative adsorption trends across different subsurface doped semiconducting oxides, which is independent of the choice of the adsorbate reference state (see the Computational Methods section for further discussion on this). Figure 1 shows the atomic structure of the (001)- BO_2 surface of STO with the subsurface substitutionally doped layer formed by replacing the Ti atoms with $3d$, $4d$, and $5d$ metals. The inset also shows the top view of the (001)- BO_2 surface, with the different binding sites. We considered adsorption on-top of the surface Ti (Host-metal (HM)) and on-top of the O for the different adsorbates. Based on our previous study [32], O, OH, and OOH preferred to adsorb on-top the Ti (HM) atom whereas H generally had a preference for the surface O site. In addition, a continuous set of other surface binding sites between the Ti and O on-top sites were covered as described in Fig. 7. We note that the thermodynamic stability of the doped STO systems considered in this study, characterized by the surface segregation energy of the dopants, has been reported in our previous work [32]. Most of the considered systems, barring a few (V, Cr, Fe, and Ru), show a preference to remain in the subsurface with positive surface segregation energies. However, it is also important not to rule out the systems that show a preference to segregate to the surface since they may be kinetically trapped in the subsurface, as evidenced by low energy ion scattering (LEIS) analysis performed on the Ru-doped STO before and after the oxygen evolution reaction

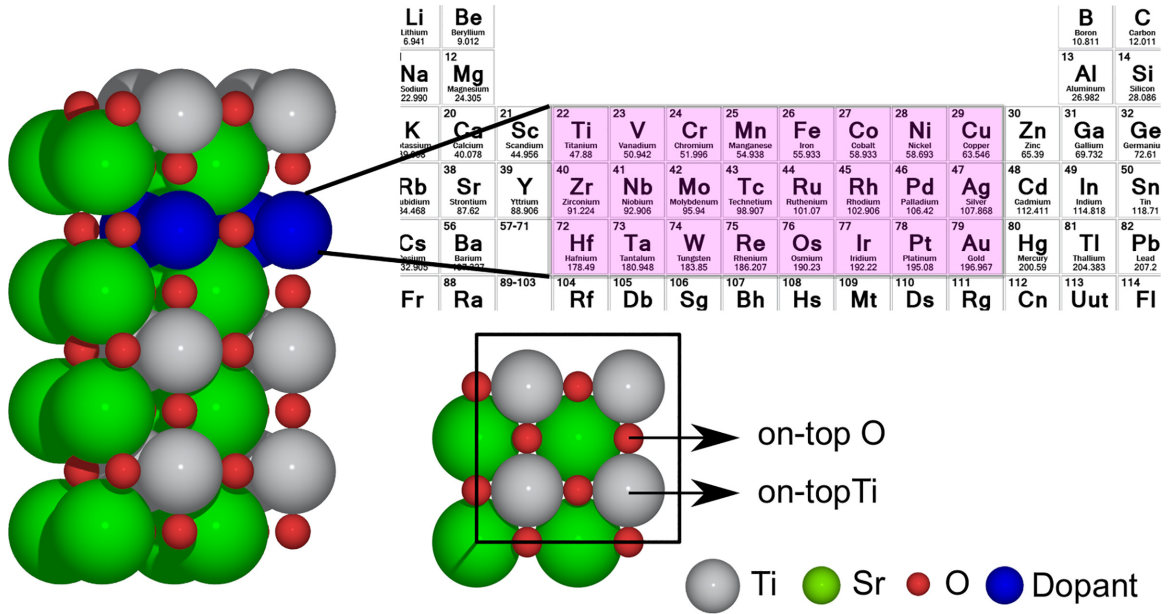


FIG. 1. Side view of the atomic structure of the (001)-BO₂ doped STO surface (STMO) used in the calculations indicating the location of the subsurface dopant layer. Top view of atomic structure of the (001)-BO₂ doped STO (STMO) surface. The highlighted region in the periodic table shows the different 3d, 4d, and 5d metals M considered as dopants in this study.

(OER) [31]. Therefore, in this study, we have considered all the systems with the dopants in the subsurface to elucidate the systematic changes to the surface electronic structure while also preserving the same surface adsorption site, viz. Ti (HM).

In order to systematically probe the influence of the electronic structure on the adsorption energy of the different adsorbates, we considered the adsorption of OH _{x} ($x = 0-1$), NH _{x} ($x = 0-2$), CH _{x} ($x = 0-3$), and SH _{x} ($x = 0-1$) on-top of the surface Ti (HM) atom. The resulting adsorbate scaling relations between the central atom (A) and the different AH _{x} species is shown in Fig. 2. We find that the expected linear relationship given by $\Delta E_{AH_x} = \gamma(x)\Delta E_A + \xi$ exists for all of the adsorbates considered, as seen with metals and other transition metal compounds [33,35]. However, a closer look at the slopes ($\gamma(x) = (x_{\max} - x)/x_{\max}$; where x_{\max} is the maximum number of H atoms that A can bind to; i.e., 2 for O and S, 3 for N, and 4 for C) reveals a more intricate surface chemistry on these oxides. For the adsorbate scaling relation between O and OH, and S and SH, we find the expected slope of 0.5 [Figs. 2(a) and 2(d)], while there is significant deviation in the slopes for the NH _{x} and CH _{x} species. The relations for N and NH and N and NH₂ are expected to scale with slopes of ≈ 0.66 and ≈ 0.33 , respectively, as found for metals, however, they instead scale with slopes of ≈ 1 and ≈ 0.5 , respectively [Fig. 2(b)], for doped STO. Similarly, we find that C and CH, C and CH₂, and C and CH₃ also scale with different slopes compared to the metals [≈ 1 , 1, and 0.5 as compared to ≈ 0.75 , 0.5, and 0.25 for metals, respectively; see Fig. 2(c)]. In addition, we considered the adsorption of OOH as well due to its importance in the OER, and found it to follow expected behavior with a slope of ≈ 0.5 (see Figs. S1 and S4 in Ref. [36]).

Similar adsorbate scaling relations as the ones identified for STMO are found for SZMO and TiMO₂ (see Figs. S4 and S3 in Ref. [36]). This suggests that the observed adsorption

trends and adsorbate scaling relations are general across different doped semiconducting oxides and not just limited to a particular host oxide. Importantly, this indicates the likely existence of a common electronic structure feature that dictates the adsorption of atoms and molecules on the surfaces of these doped semiconducting oxides.

B. Electronic structure analysis

We next perform a detailed electronic structure analysis which will provide key observation that will serve as the basis for our adsorption model development. We emphasize our discussion around the following topics: (1) the role of the different adsorbates on perturbing the electronic structure of the oxide, (2) how the adsorbate geometry influences the electronic structure, and (3) how the adsorption site affects the binding of the adsorbate through the lens of the electronic structure. The outcomes of the analysis are a set of hypotheses to be considered for the model construction.

1. Perturbation to the electronic structure due to the adsorbate

We first considered the electronic structure of the adsorbate states in their geometry optimized positions on the (001)-BO₂ surface of undoped pristine STO. Figure 3 shows the projected density of states (PDOS) of the different adsorbates; specifically, the O-2p, S-3p, N-2p, and C-2p states for adsorption on-top the surface Ti site and the H-1s for adsorption on-top the surface oxygen site. Considering the PDOS of the adsorbates on-top the surface Ti site of the undoped STO surface, it can be seen that there are distinct differences. For example, going from C to O, the bonding peaks are shifted lower down in energy, with both C and N having bonding states that are partly unoccupied as they cross the Fermi level, while for S and O, they are just below the Fermi level. On the other hand, H adsorbed on-top the O has a bonding state that is very low

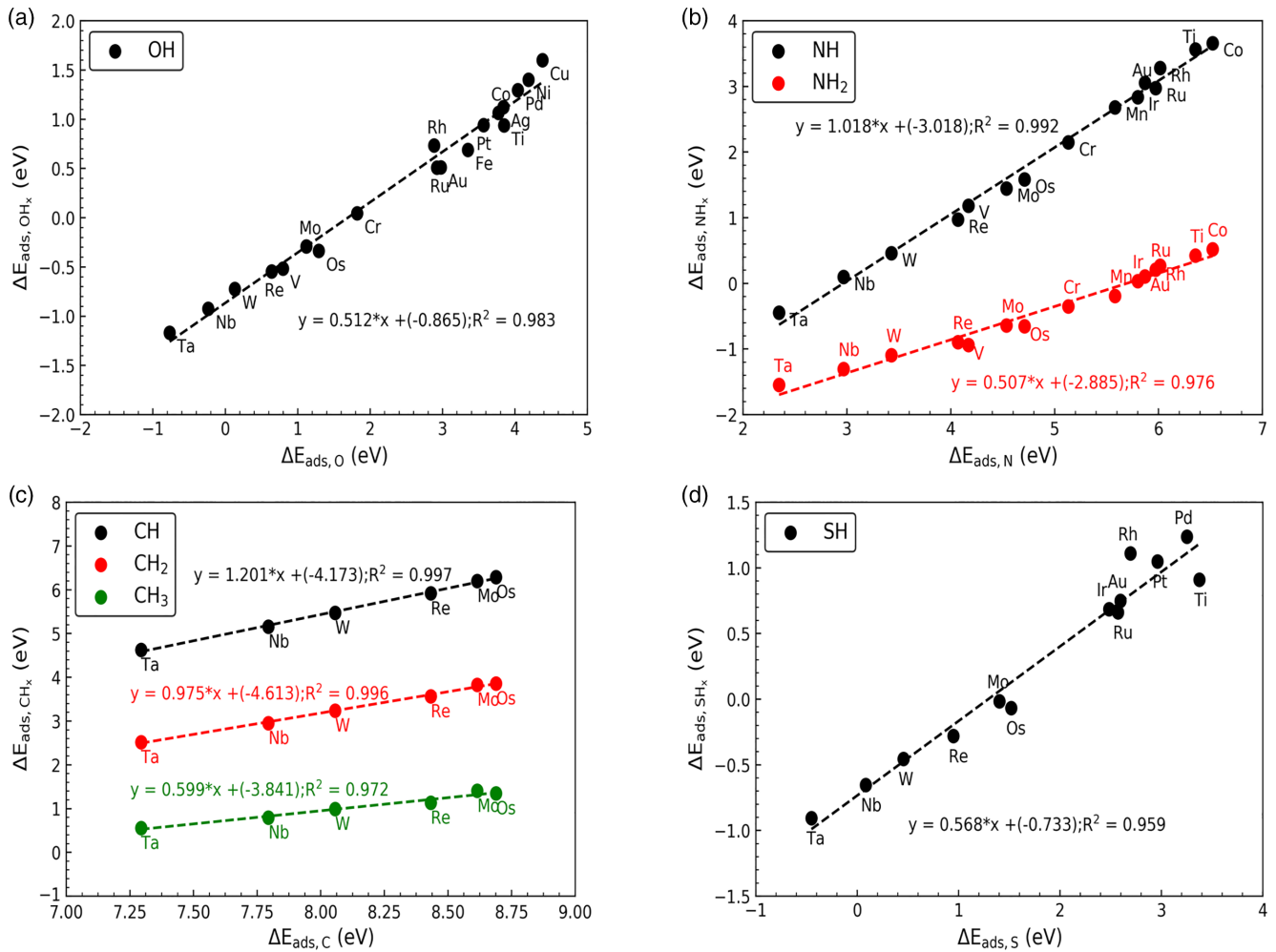


FIG. 2. Adsorbate scaling relations between the central atom (A) and the different AH_x species for adsorption on-top the surface Ti atom of the (001)- BO_2 surface of STMO for (a) OH_x ($x = 0-1$), (b) NH_x ($x = 0-2$), (c) CH_x ($x = 0-3$), and (d) SH_x ($x = 0-1$). M corresponds to $3d$, $4d$, and $5d$ transition metals doped in the subsurface of STO.

in energy (≈ -7.5 eV), as well as a completely unoccupied antibonding state above the Fermi level, indicating a much stronger bond. We will first consider the adsorption on-top the Ti-atom followed by that on-top the O atom.

In order to decipher the changes to the electronic structure of the surface Ti and O atoms induced by the presence of the adsorbate, we computed the Δ PDOS of the Ti- $3d$ and O- $2p$ states with and without the adsorbate; i.e., Δ PDOS = PDOS(Ti- $3d$ and O- $2p$ /ads) - PDOS(Ti- $3d$ and O- $2p$, clean surface). The Δ PDOS for STO due to the adsorption of O, N, C, and S on-top the surface Ti atom is shown in Fig. 4. The positive Δ PDOS states refer to those that have been formed due to adsorption and the negative Δ PDOS refer to the states that have been shifted relative to the clean surface. Despite adsorption on-top of the Ti atom, it is clear that there is a hybridization between the surface oxygen states (green) and the adsorbate states (red) as well, potentially implying that all of the surface atoms play a role in the adsorption to some extent, irrespective of the adsorption site. This is especially prominent with the bonding state of O, N, and S, and to some extent C as well, with the antibonding states above the Fermi level typically dominated by the Ti- $3d$ states (blue).

We also note that between O, N, and C, in addition to the shift in the position of the bonding states, there is a difference in the split between the bonding and antibonding states, which is even more pronounced as evident in Fig. 4. The largest split is seen for O, followed by N, and finally C with the smallest split. S does not show a distinct adsorbate antibonding state but based on the position of the bonding states and the newly formed Ti- $3d$ states, the split is expected to be somewhere between O and N. This is a consequence of the different coupling strengths (V^2) between the adsorbate and the surface atoms (particularly the Ti atom), as a result of the different optimal bond lengths at which these adsorb on the surface. The optimal bond length for O, N, and C is found to be ≈ 1.65 , 1.80 , and 2 Å (i.e., $O < N < C$), respectively, relative to the surface Ti atom adsorption site. Since the coupling strength generally varies inversely with distance, this implies that $V_{Ti,Oads}^2 > V_{Ti,Nads}^2 > V_{Ti,Cads}^2$ as a first-order approximation, which results in the largest split between the bonding and antibonding states for O and the smallest for C. While we may have expected that an adsorbate which is more electron rich (i.e., O) would require a lower optimal electron density when adsorbed on the surface, which

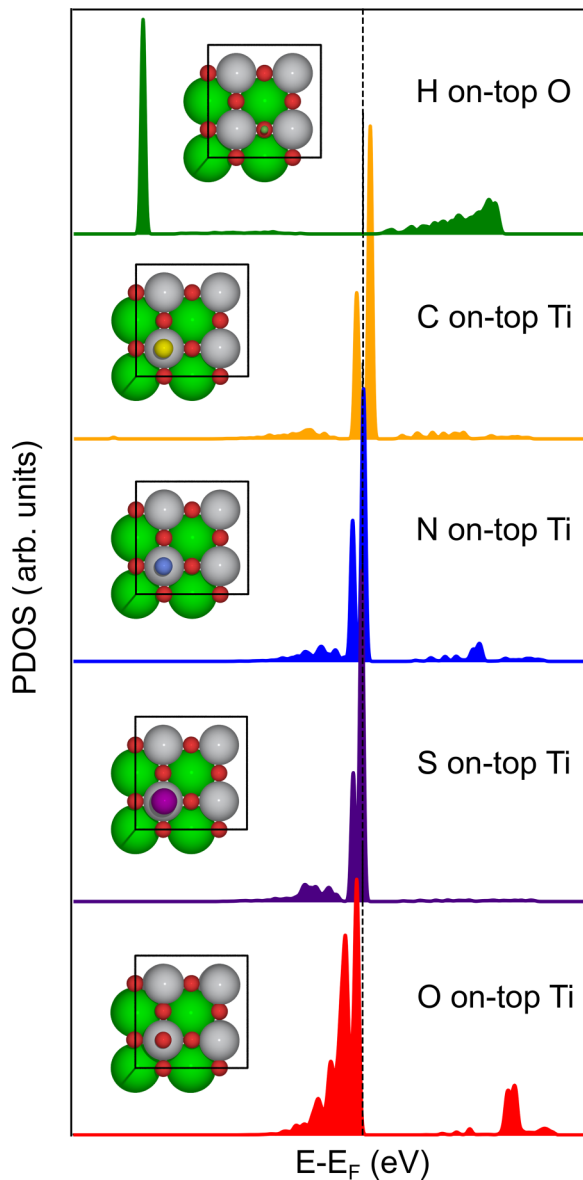


FIG. 3. The projected density of states (PDOS) of the different adsorbates in their most favored geometry optimized position on the (001)-BO₂ surface of undoped STO. From top to bottom: H-1s (adsorbed on-top of O); C-2p, N-2p, S-3p, and O-2p (adsorbed on-top of Ti) states. The corresponding adsorbed configurations on the preferred surface sites are shown in the insets, and the vertical dashed line corresponds to the Fermi level.

would be encountered further away from the surface based on a simplistic approach such as the effective medium theory (EMT) [37], we observe the opposite trend here. This coupled with the concerted nature of the coupling between the adsorbate and the surface atoms therefore requires the development of an adsorption model beyond those that have been developed for metals such as the *d*-band model [29], which primarily relies on a single electronic structure feature. We hypothesize that an adsorption model for oxide surfaces needs to build around more than one electronic structure feature to account for the observed concerted coupling in the complex systems.

To build an adsorption model for oxides, we first modify the system in a controlled way by perturbing the electronic structure of the surface atoms of the host oxide through the addition of metal dopants to the subsurface to establish the resulting unique trends in the adsorption energy. Simultaneously, we also note that adsorbate induced changes to the PDOS demonstrate shifts in the bonding and antibonding states across the different doped host oxides that can be used to better understand the adsorption energy trends (see Figs. S5–S19 in Ref. [36]). In the forthcoming sections, we will therefore use these unique features to quantify the changes to the adsorption energy due to changes in the electronic structure through a set of targeted *in silico* experiments.

2. Role of adsorption geometry on the electronic structure

The first set of *in silico* experiments that we performed involves probing the effect of the coupling strength between the adsorbate and the surface starting with the on-top Ti adsorption site. We considered the geometry optimized structures with the adsorbate (O for illustration) and then moved the adsorbate both outward and inward along the surface normal ($d_z = +0.3$ and -0.3 Å, respectively) corresponding to decreasing and increasing coupling strengths, respectively. Figure 5 shows the Δ PDOS of the surface and dopant layer atoms along with the changes in the O adsorbate states at different distances away from the surface Ti atom for Mo-doped STMO. We note that similar effects are seen across the different adsorbates and different dopants, with the Mo-doped system shown here for illustrative purposes (see Figs. S20 and S21 in Ref. [36] for the other doped STMO systems). It can be seen that relative to the geometry optimized case, increasing $V_{\text{Ti,Oads}}^2$ (i.e., $d_z = -0.3$ Å relative to the geometry optimized position) results in a much larger split between the bonding and antibonding O adsorbate states, with the bonding peak especially pushed to lower energies (≈ -6 eV compared to ≈ -2 eV below the Fermi level). Decreasing $V_{\text{Ti,Oads}}^2$ (i.e., $d_z = +0.3$ Å relative to the geometry optimized position) results in a much smaller split between the bonding and antibonding O adsorbate states, with the bonding states pushed very close to the Fermi level.

The corresponding adsorption energy trends across the 4*d* dopants in STO are shown in Fig. S39 in Ref. [36]. Both increasing and decreasing the coupling strength results in a weaker adsorption energy relative to the optimum, however, for differing reasons. With decreasing coupling strength, the adsorbate bonding states are shifted to higher energies closer to the Fermi level resulting in an increase in the overall adsorption energy, while with increasing coupling strength, repulsion starts to dominate resulting in weaker adsorption. It can also be seen from Fig. 5 that there is a quenching of the dopant states (brown) in the vicinity of the Fermi level, suggesting a charge transfer from the dopant layers to the newly formed adsorbate bonding state, which is confirmed through a Bader charge analysis (see Tables S3, S4, and S5 in Ref. [36]). Further, we note that such a charge transfer does not occur in undoped STO, where the surface O contributes the maximum amount of charge. Additionally, irrespective of the dopant, for a given position of the O adsorbate above the surface, the charge gained by the adsorbate is roughly constant

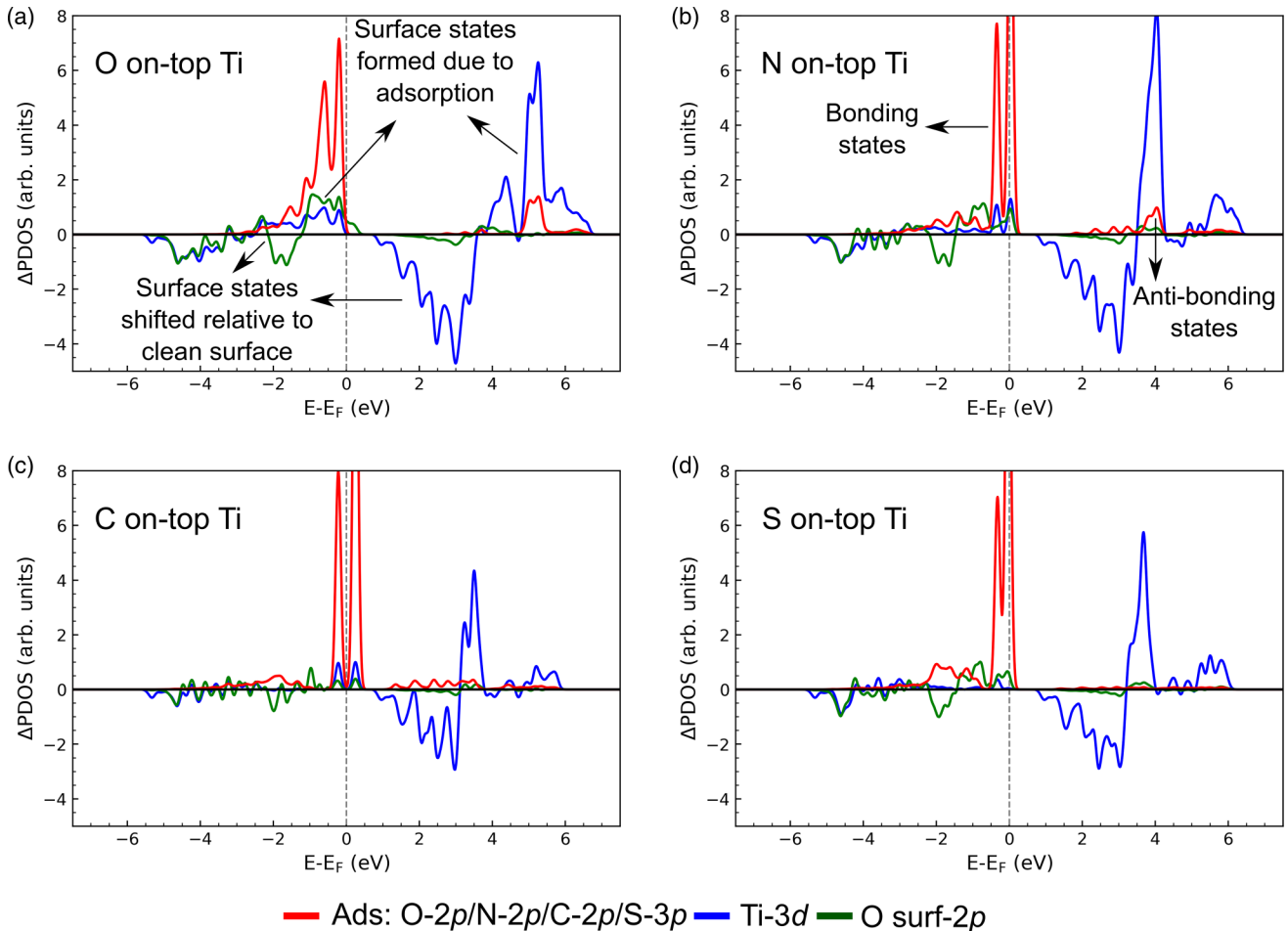


FIG. 4. Δ PDOS of the Ti-3d and O-2p states of the surface atoms of the (001)-BO₂ surface of STO induced by the presence of different adsorbates. The corresponding adsorbate states are also shown: (a) O-2p, (b) N-2p, (c) C-2p, and (d) S-3p.

($\approx -0.5e$ to $-0.6e$). The charge transfer from the dopant layer, and the equal charge on the adsorbate, were also seen in our previous study and formed the basis for the tuning mechanism proposed for improving the OER activity [32]. We hypothesize that despite the position of the adsorbate above the surface, the participation of the dopant states may be due to the resultant hybridization in the original geometry optimized system, where we also observed an upward translation of the Ti atom on which the O adsorbs.

In order to disentangle the effect of the surface geometry on the adsorption, we adsorbed O on a constrained surface, allowing only the adsorbate to relax on the surface. The geometry optimized and surface constrained Δ PDOS due to the adsorption of O on-top of the Ti adsorption site of Ru-doped STMO is shown in Fig. 6 as an example. We can see that while the features of the geometry optimized Δ PDOS are similar to the ones discussed above for the Mo-doped STMO system, the surface constrained Δ PDOS shows different features. Specifically, the bonding state is shifted higher up in energy and also crosses the Fermi level (weaker coupling; larger bond lengths on average ≈ 1.8 to 1.9 Å), and the large negative peaks of the dopant states in the vicinity of the Fermi level seen with the geometry optimized case are now absent. There are also significant surface O-2p states that hybridize with the O adsorbate 2p states as seen with the bonding peak.

This is also reflected in the Bader charges shown in Table S6 where the charge given by the dopant layer is ≈ 0 , with the maximum amount of charge given by the surface O atoms to the adsorbate, as observed for undoped STO. The charge gained by the adsorbate is no longer a constant across the different dopants, with O adsorbed on the Nb doped system gaining the maximum charge ($-0.49e$) and Ag getting the least ($-0.31e$). This is as a result of the bonding states shifting across the Fermi level as we move across the period from left to right due to the weaker coupling between the O adsorbate and Ti states, with the Fermi level itself pinned by the dopant. We note that a similar effect is observed for both N and C adsorbed on the surface Ti atom even for the geometry optimized case (see Figs. S9 and S12 in Ref. [36]), presenting a distinct deviation from that of O. Taken together, this suggests that the charge density above the surface is largely set by the surface O-2p states, which in turn dictates the optimal bond length for a given adsorbate (and therefore the coupling strengths), which in turn affects the position of the resultant adsorbate bonding and antibonding peaks. We also note that based on the position of the resulting bonding state of the adsorbate, there is a charge transfer from the dopant states at the Fermi level, for adsorption on the surface Ti (host-metal) atom. The role of the different surface sites and the quantification of the changes to the adsorption energy by the perturbation of the

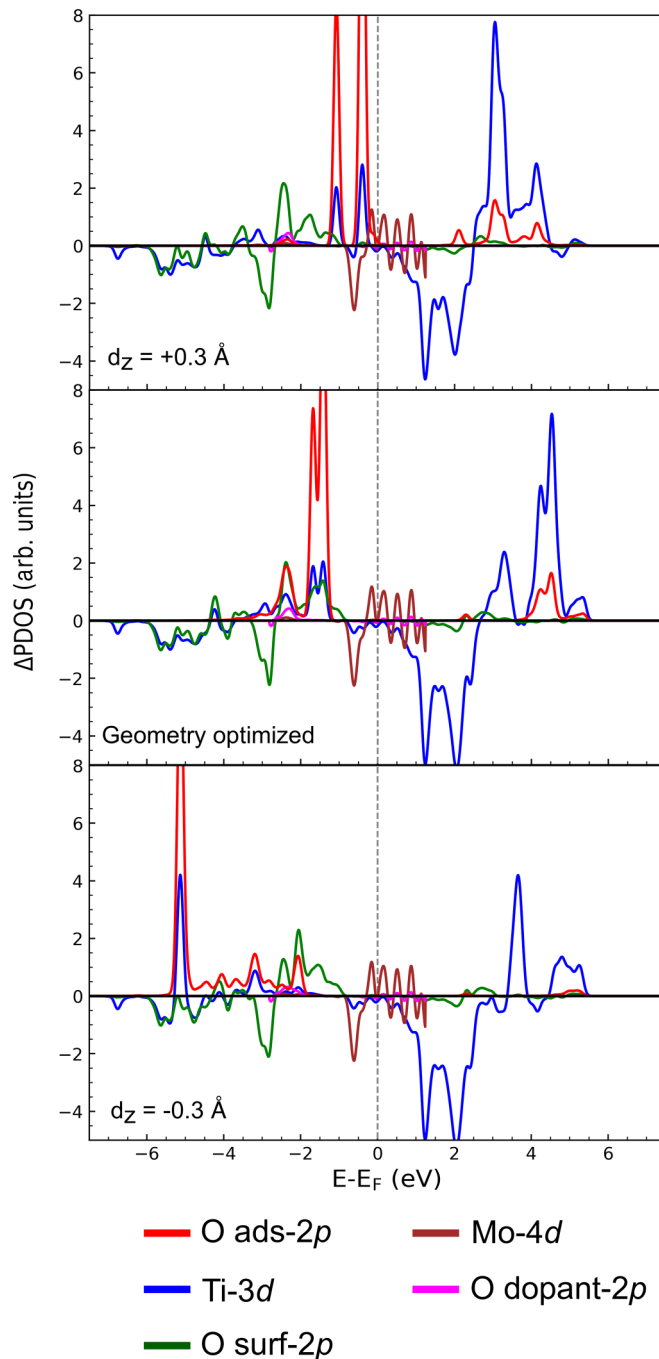


FIG. 5. Δ PDOS of the Ti-3d and O-2p states of the surface atoms of the (001)-BO₂ Mo-doped STMO surface induced by the presence of the adsorbate (O) at different distances above the surface Ti atom adsorption site. The corresponding adsorbate states, as well as the Δ PDOS of the dopant states (subsurface Mo and O) are also shown.

electronic structure due to the addition of dopants is discussed in the next two sections.

3. Role of the surface adsorption sites on the binding of different adsorbates

To decipher the contributions of the surface Ti (HM) and O atoms to the adsorption energy of the different adsorbates,

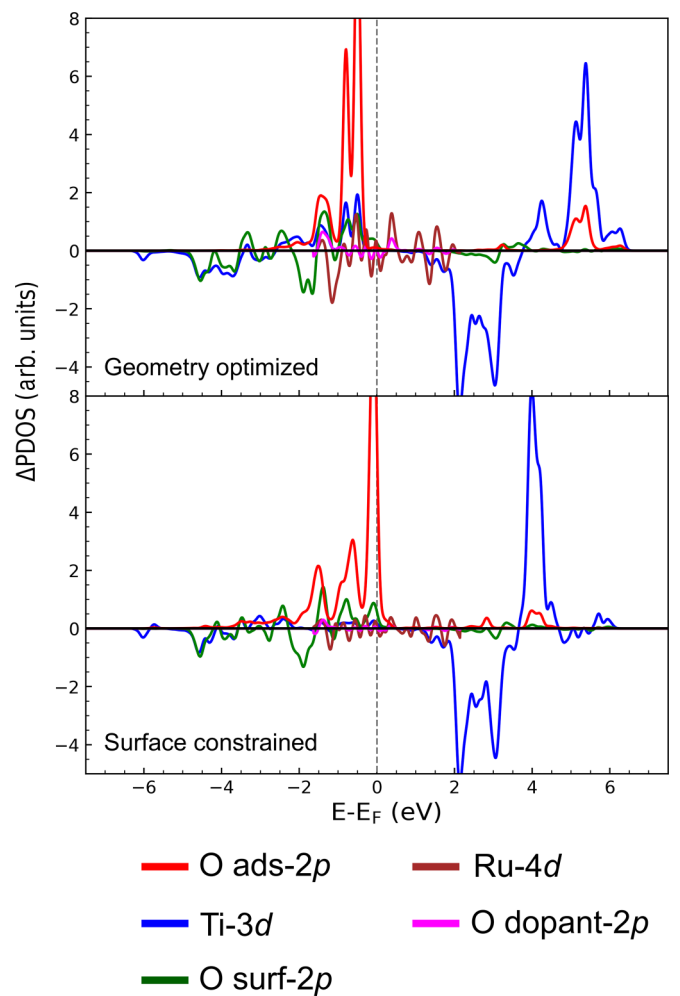


FIG. 6. Δ PDOS of the Ti-3d and O-2p states of the surface atoms of the (001)-BO₂ surface of STO doped with Ru induced by the presence of the adsorbate (O), for the geometry optimized case (top) and with the constrained surface (bottom). The corresponding adsorbate states, as well as the Δ PDOS of the dopant states (subsurface Ru and O) are also shown.

we performed the following set of *in silico* experiments. First, we computed the 2D charge density and electrostatic potentials at ≈ 1.5 Å above the surface, as shown in Fig. S32 in Ref. [36]. The regions of higher charge density are around the surface O atoms, with the magnitudes of the charge density roughly constant across the different 4d dopants in STMO, as well as undoped STO. This is due to the localization of the charge in the dopant layer in these systems as reported in our previous studies [31,32]. Note that this observation is a stark contrast to near surface alloys of metals where there is expected to be a charge transfer from the subsurface to the surface atoms based on the difference in electronegativities of the metals making up the alloy [38]. This is expected to also affect the charge density above the surface and therefore also the optimal bond lengths and coupling strength between the adsorbate and surface atoms [38]. However, we note that as hypothesized in the previous section, the charge density above the surface is largely set by the surface oxygen atoms and is largely unaffected by the presence of the dopants in

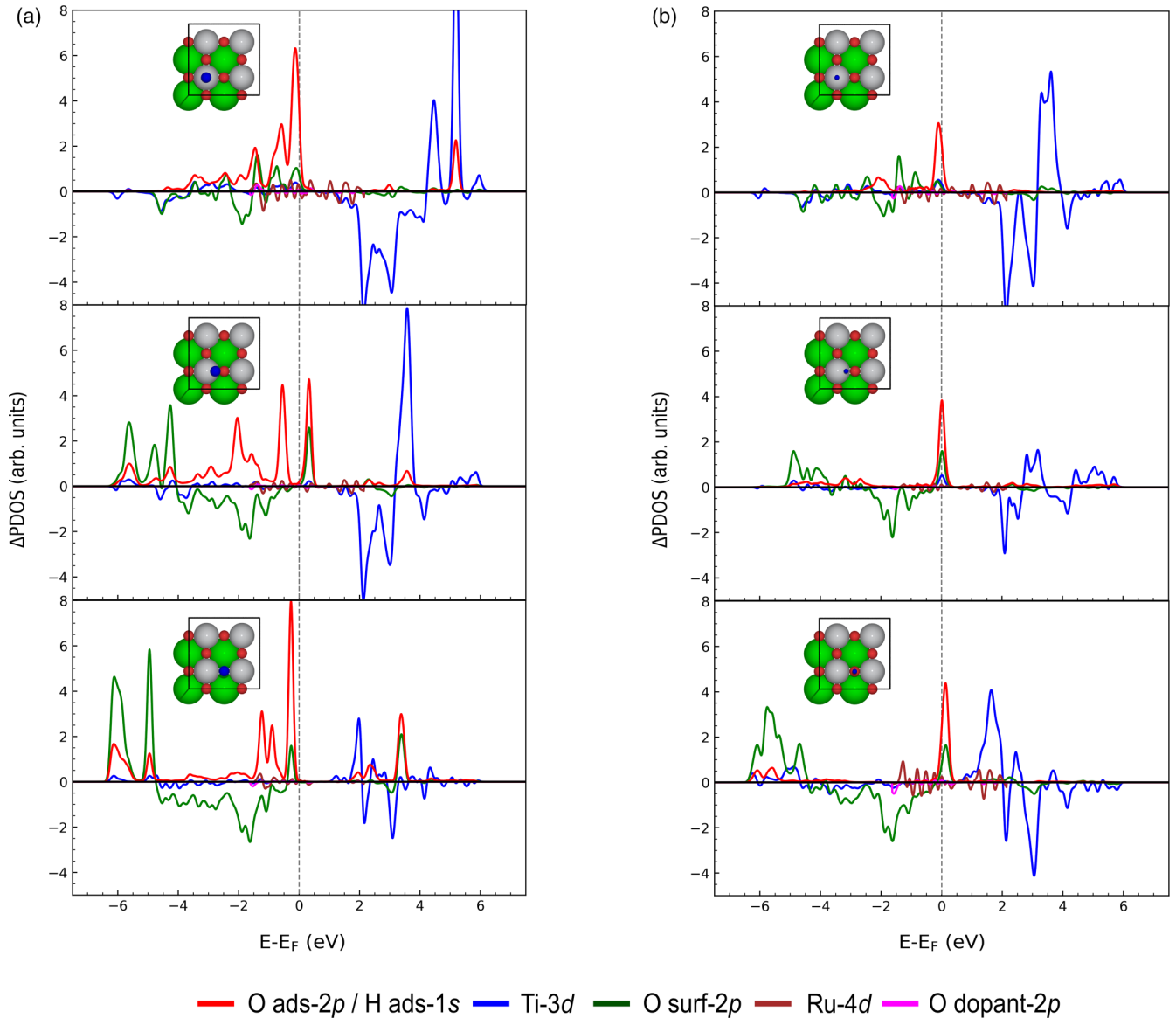


FIG. 7. Δ PDOS of the Ti-3d and O-2p states of the surface atoms of the (001)-BO₂ surface of Ru-doped STMO induced by the presence of the adsorbates (a) O and (b) H, when moved across the surface at a fixed distance above the surface (from top to bottom: Ti-top, in-between Ti and O, and O-top). The corresponding adsorbate states, as well as the Δ PDOS of the dopant states (subsurface Ru and O) are also shown. Inset shows the top view of the adsorption configurations. Color codes: Ti-grey, O surface-red, Sr-green and adsorbate (O or H): blue.

the subsurface. This also explains the generally constant bond length for each adsorbate across all the doped systems as well as the undoped host, implying that the coupling strength ($V_{\text{HM,ads}}^2$ and $V_{\text{O,ads}}^2$) is largely set by the undoped host oxide.

Next, we considered the adsorbate specific influence of the different surface binding sites by comparing the O and H adsorbate, where it is known from previous studies [32] that O generally prefers to adsorb on-top the Ti (HM) site and H on-top the surface O site. We placed the O and H adsorbates at their optimized bond lengths above the surface Ti atom of the pristine STO optimized surface and performed calculations where the adsorbates were moved across to the nearest oxygen atom at the same distance above the surface. This is illustrated in Fig. 7, along with the Δ PDOS at each location above the surface (Ru-doped STMO is shown as

an example; see Figs. S22–S27 in Ref. [36] for the other doped STMO systems). Whereas in the previous section, we explored the influence of the coupling strength with respect to just the Ti atom, the concerted nature of the coupling necessitates the investigation of the relative coupling strengths between the surface Ti and O atoms and the adsorbate (i.e., $V_{\text{HM,ads}}^2$ versus $V_{\text{O,ads}}^2$), which is achieved by the above experiment.

We observe distinct differences in the Δ PDOS for each adsorbate across the three adsorption sites (Fig. 7), as well as between the two adsorbates O and H. Generally we find that as the adsorbate is moved across from the Ti to the O surface atom, there is an increase in hybridization between the adsorbate and the O atoms, seen with the newly formed bonding states at much lower energies (< -5 eV) below the

Fermi level dominated by the surface O-2*p* states, for both O and H. This instantly reflects the higher coupling strength between the adsorbate and surface O (i.e., $V_{O,ads}^2 \gg V_{HM,ads}^2$), as we move across from the Ti-top to the O-top adsorption site. The biggest difference in the Δ PDOS between the adsorbates is the appearance of localized (nonbonding) states in the vicinity of the Fermi level for O in addition to the bonding and antibonding peaks below and above the Fermi level, respectively. For H on the other hand, the bonding peak just below the Fermi level starts to shift above the Fermi level and first becomes partly unfilled when adsorbing in between the Ti and O atoms, and completely unfilled for adsorption on-top of the O atom. This is simultaneously accompanied by the formation of bonding states in the lower valence band well below the Fermi level. This is reflected in the Bader charges for O and H calculated for these three adsorption sites (see Tables S7, S8, and S9 for O adsorbed on-top Ti, in-between and on-top O, respectively; and Tables S14, S15, and S16 for H adsorbed on-top Ti, in-between, and on-top O, respectively, in Ref. [36]).

For the O adsorbate, the charge on the adsorbate remains negative (i.e., charge gain) irrespective of the adsorption site, although there is a slight decrease in the amount of charge gained (≈ -0.1 e decrease). As discussed in the previous section, the surface O atoms are involved in the largest charge transfer to the adsorbate irrespective of the adsorption site. On the other hand, H goes from accepting charge from the oxide when adsorbed on-top the Ti atom to giving charge to the oxide when moved over to the surface O atom (for the Ru-doped STMO; -0.19 e on-top Ti; and $+0.13$ e on-top O). We note that this change is also commensurate with the dopant in the host oxide, and the corresponding shifts in the bonding and antibonding peaks relative to the Fermi level pinned by the dopant (for example, in Nb-doped STMO; H on-top Ti has a computed Bader charge of -0.33 e and -0.01 e for H on-top O). Taken together, there is charge transfer between the surface O atoms and H adsorbate (with the dopant layer also receiving some charge when H adsorbs on-top of the surface O). All of this is reflected in the adsorption energy trends shown in Figs. S40 and S41 in Ref. [36] for O and H, respectively. For O, the adsorption energy becomes almost equal across all the dopants, and equivalent to that of undoped STO when moved to the on-top O adsorption position from the on-top Ti position, where the characteristic “check-mark” shape is seen with Nb-doped STMO having the lowest adsorption energy. For H, while the check-mark shape is seen for adsorption on the Ti atom, it changes to an inverse ‘check-mark’ shape for the adsorption on-top of the O atom, with Nb and Mo having the higher adsorption energies and Ag the lowest. Therefore we hypothesize that the relative coupling strength between the surface Ti (HM) and O; and the adsorbate, as well as the adsorbate state are intrinsically related through the adsorption site and the electronegativity of the adsorbate itself (through their electron-affinity (or ionization energy)) as has been suggested previously [39]. This becomes evident from the discussion above involving the distinct differences between two adsorbates (H and O) of disparate electronegativities and their adsorption on the different surface sites. Additionally, we have now established that changes to the surface states by the addition of dopants to

the subsurface also couples to this, giving an overall concerted coupling of the adsorbate and the surface. A similar adsorption energy trend (reverse check-mark shape) is also seen for the geometry optimized case involving H adsorption on the O atom [32]. Further, the Bader charges on the H adsorbate are also found to be positive (implying that it gives charge to the oxide) and constant ($\approx +0.65$ e) across all the doped systems with STMO as well as undoped STO. However, based on the observations of the Δ PDOS for H adsorption on the surface O atom (see Fig. S8 in Ref. [36]), Nb which has the bonding peak at a lower energy (≈ -8.5 eV, as well as a completely unfilled antibonding state), and therefore lower one-electron energies also has the highest(weaker) adsorption energy compared to Ag which has the lowest (bonding peak at ≈ -5.5 eV), similar to the trends discussed above. This therefore gives a distinct new adsorption mechanism involving adsorption on-top the surface O atom for adsorbates with lower electronegativity that tend to ionize such as hydrogen. Therefore we can now classify the adsorption into two distinct categories as electron-accepting and electron-donating based on a combination of the adsorbate electronegativity and the adsorption site (i.e., O/N/C/S on Ti-top: electron-accepting and H on O-top: electron donating). Armed with the observations made in the above sections, we now proceed with the development of the adsorption model.

C. Adsorption model

1. Quantifying the hybridization energy

In order to quantify the concerted coupling nature of the adsorption established through the electronic structure analysis and its influence on the adsorption energy, we used the Newns-Anderson model [40,41] to compute the hybridization energy on STMO. We focus our analysis on the STMO with M corresponding to 4*d* transition metals doped in the subsurface for the case of the electron-accepting adsorption (i.e., adsorption on the surface HM atom). The Newns-Anderson model is discussed in detail in the Computational Methods section along with the pertinent equations. Briefly, we considered the adsorbate defined by its ‘free’ adsorbate state (ϵ_a) to interact independently with the surface Ti-3*d* and O-2*p* states which gives the overall hybridization energy, as defined by Eq. (18). The changes to the Ti-3*d* and O-2*p* surface states due to the addition of the dopants was modeled through a semiellipse fit of the corresponding PDOS (Ti-3*d* and O-2*p*) of undoped STO, as shown in Fig. S30 in Ref. [36]. We note that there is no change to the filling of the surface Ti-3*d* and O-2*p* states due to the addition of dopants (see Fig. S31 in Ref. [36]) but only a shift in the corresponding band centers (see Fig. S42d in Ref. [36]). This allowed us to construct the semiellipse fit by preserving the centers of both the valence band (VB) and conduction band (CB), as well as the filling, with respect to the DFT computed PDOS of undoped STO. Further, a “rigid-shift” model of the semiellipse fit PDOS was used, by translating the O-2*p* and Ti-3*d* states independently over the relative energy scale to approximate the changes to the surface electronic structure caused by the addition of dopants to the subsurface. For a fixed ϵ_a , we considered three distinct possibilities involving the relative coupling strengths

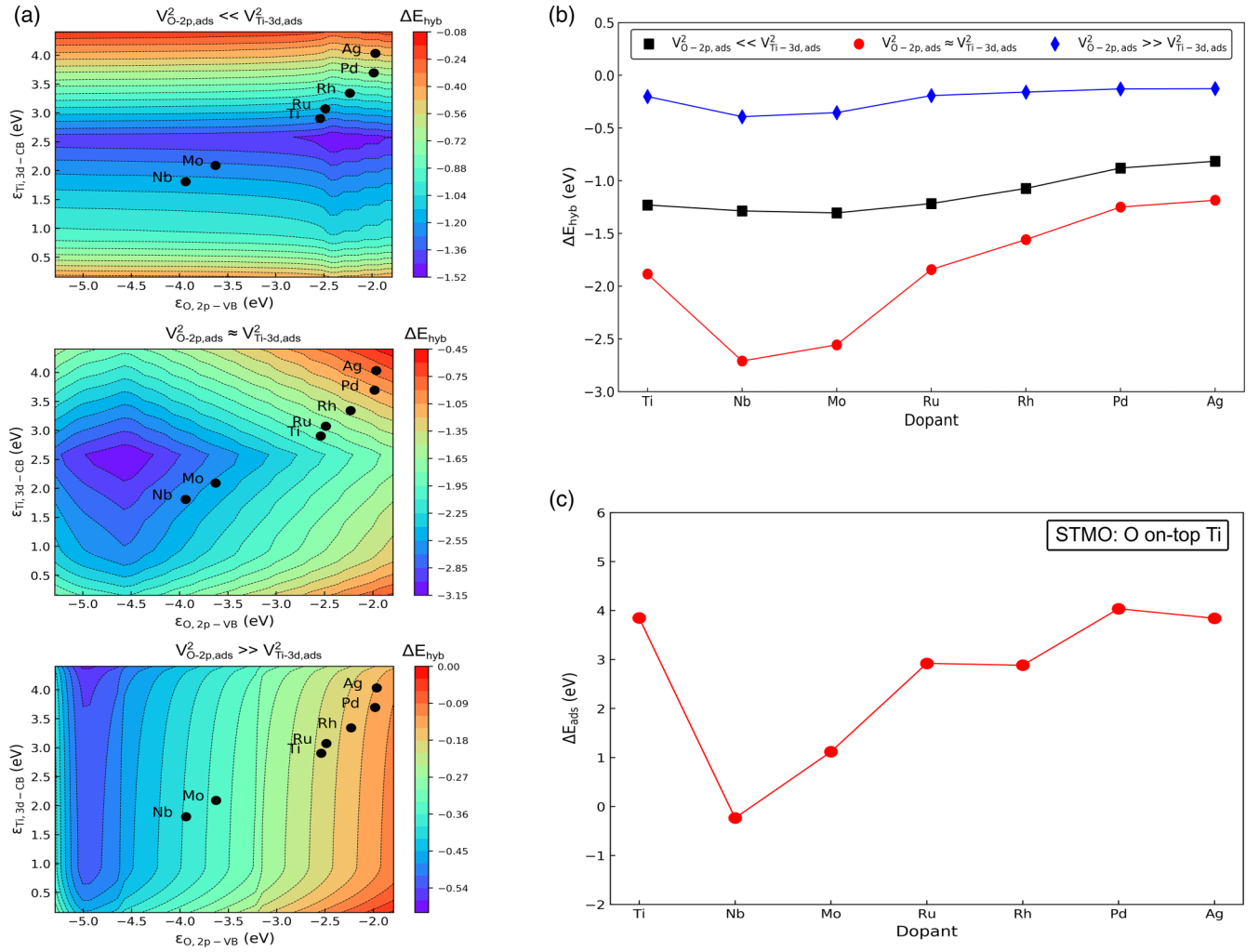


FIG. 8. Calculated hybridization energy (ΔE_{hyb}) using the Newns-Anderson model and two semiellipse fits for the PDOS; one for the surface Ti and the other for the surface O atoms of STO. The 2D heat map of ΔE_{hyb} as a function of varying positions of the O-2p valence band (VB) and Ti-3d conduction band (CB) for a given adsorbate state (ϵ_a) and different relative coupling strengths between the adsorbate and surface O and Ti atoms. (a) Strong Ti coupling (top), comparable concerted coupling (middle) and strong O coupling (bottom). (b) ΔE_{hyb} for the different 4d transition metal doped STMO as well as the undoped STO computed using the Newns-Anderson model for the three different relative coupling strengths. (c) DFT computed O adsorption energy with adsorption on-top of the surface Ti atom of 4d transition metal doped STMO.

between the Ti-3d and O-2p states, and the adsorbate: (i) a strong coupling between the Ti-3d states and the adsorbate, (ii) a strong coupling between the O-2p states and the adsorbate, and (iii) a comparable concerted coupling between both the Ti-3d and O-2p states and the adsorbate. We also note that in our analysis, since ϵ_a is fixed to be a constant, the $n_a \epsilon_a$ contribution to the hybridization energy in Eq. (18) can be factored out for a given adsorbate.

The results from the three coupling cases are discussed next. The calculated hybridization energy (ΔE_{hyb}) is shown in the form of a 2D heat map [see Fig. 8(a)] as a function of the surface O-2p valence band center ($\epsilon_{\text{O},2p-\text{VB}}$) and surface Ti-3d conduction band center ($\epsilon_{\text{Ti},3d-\text{CB}}$). These centers are chosen since the VB is dominated by the O-2p states and CB by the Ti-3d states. Note that the total band centers VB+CB could also be used equivalently since the band-gap is a fixed constant. The corresponding DFT computed O-2p-VB and

Ti-3d-CB band centers for the different doped STMO systems, as well as that of undoped STO are overlaid on the 2D heat map. For $V_{\text{O}-2p,\text{ads}}^2 \ll V_{\text{Ti}-3d,\text{ads}}^2$, i.e., the case where there is a much stronger coupling between the surface Ti-3d states and the adsorbate [see Fig. 8(a)], we find that the contour lines are almost parallel to the x axis ($\epsilon_{\text{O},2p-\text{VB}}$), meaning that ΔE_{hyb} is varying in magnitude largely with changes in the position of $\epsilon_{\text{Ti},3d-\text{CB}}$ while being nearly independent of the changes in $\epsilon_{\text{O},2p-\text{VB}}$. On the other hand, for $V_{\text{O}-2p,\text{ads}}^2 \gg V_{\text{Ti}-3d,\text{ads}}^2$, i.e., a strong coupling between the O-2p states and the adsorbate, we find that the contour lines are positioned almost parallel to the y axis ($\epsilon_{\text{Ti},3d-\text{CB}}$), meaning that the largest variations in ΔE_{hyb} are due to the position of $\epsilon_{\text{O},2p-\text{VB}}$ while being nearly independent of $\epsilon_{\text{Ti},3d-\text{CB}}$. Finally, for the case where there is a concerted coupling between the adsorbate and both the Ti-3d and O-2p surface states, we consider a comparable coupling strength, i.e., $V_{\text{O}-2p,\text{ads}}^2 \approx V_{\text{Ti}-3d,\text{ads}}^2$ with a slightly

lower $V_{O-2p,ads}^2$ value to reflect the adsorption geometry being on-top of surface Ti atom for an electron-accepting adsorbate. This coupling scenario results in a well-defined minimum in ΔE_{hyb} that corresponds to the strongest adsorption, and is importantly seen to be a function of the position of both $\varepsilon_{O-2p-VB}$ and $\varepsilon_{Ti-3d-CB}$. The contour lines also reflect this complex dependence resulting in a concerted contribution to the adsorption energy where the adsorbate interacts with both the Ti and O surface atoms.

The hybridization energies corresponding to the different doped systems indicated in the 2D heat-map [Fig. 8(a)] are plotted in Fig. 8(b). We find that for the two extreme cases involving the very strong coupling of either the Ti-3d (black) or O-2p (blue) states and the adsorbate, ΔE_{hyb} is nearly a constant across all of the 4d dopants as well as the undoped STO. However, for the concerted coupling case (red), we obtain the distinct check-mark shape across the period with Nb having the lowest and Ag the highest ΔE_{hyb} values. This should be directly compared to the DFT calculated adsorption energy trends for the electron-accepting adsorption, as shown for O adsorption on-top of the surface Ti atom [see Fig. 8(c)]. We note that while the absolute numbers are different between the two, i.e., calculated using the concerted coupling scenario of the Newns-Anderson model [ΔE_{hyb} , see red circles in Fig. 8(b)] versus the DFT computed adsorption energies [see Fig. 8(c)], this is expected due to two things. First, we have not explicitly included the repulsive contribution in the Newns-Anderson model and second the values used for the coupling strengths and the adsorbate state in our model are approximate values intended to only distinguish the different limiting cases. However, we note that the addition of the repulsive contribution would only result in a linear shift of ΔE_{hyb} by an amount roughly proportional to the coupling strength. Thus we can expect the adsorption energy trend to be the same albeit with different absolute values. Therefore the intention of employing the Newns-Anderson model is not to get quantitative agreement with DFT computed adsorption energies but rather establish fundamental insights into the adsorption process and obtain qualitative trends. Based on the analysis presented here, it is clear that the concerted coupling of both the surface Ti-3d and O-2p states with the adsorbate contributes to the adsorption, as observed in the computed $\Delta PDOS$ and hypothesized in the previous section. Using this insight, we now proceed with presenting the adsorption model hitherto referred as the GCC model and identify a general electronic structure based descriptor that captures the adsorption energy trends.

2. The generalized concerted coupling model

We utilized the insights obtained in the previous section (note the indicated key findings and hypothesis) to develop an adsorption model called the generalized concerted coupling model that is found to be applicable to subsurface doped semiconducting oxides. We will focus on the electron-accepting adsorption (i.e., adsorption of, e.g., O on-top of the surface Ti (HM) atom) on the prototype STMO system to develop this model. It is evident from the discussion above that the dopant induced changes to the electronic structure of the surface atoms plays a crucial role in the adsorption process

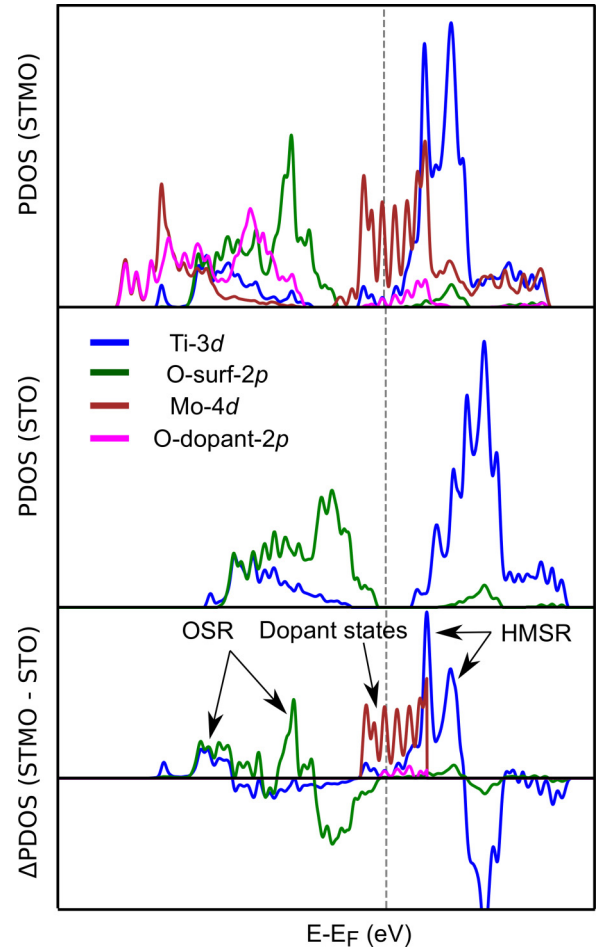


FIG. 9. $\Delta PDOS$ of the surface Ti-3d and O-2p states, as well as the dopant states in the gap, computed by taking the difference between the PDOS of the oxide with the dopant (STMO) and without the dopant (STO). The Mo-doped STMO system is shown here as an example. The surface resonance states are indicated as OSR and HMSR. The vertical dashed line corresponds to the Fermi level.

as well as the type of charge transfer between the dopant states and the adsorbate. To quantify these changes to the surface states, we computed the $\Delta PDOS$ of the surface Ti-3d and O-2p states with the dopants (STMO) and without dopants (STO), i.e., $\Delta PDOS = PDOS(STMO) - PDOS(STO)$. One example of this difference in PDOS is shown in Fig. 9 for the Mo-doped STMO system. We find that addition of dopants results in the formation of distinct features in the surface Ti-3d and O-2p states, with the positive peaks indicating the new positions of the states as a result of the addition of Mo. Since these states overlap in energy with the PDOS of the surface atoms, they are termed surface resonance states. These type of state are similar to those that have been observed in transition metal carbides and nitrides [42,43] as well as doped oxides [44]. For the Mo-doped STMO, we find that the valence band is dominated by the O-2p surface resonances (OSR) and the conduction band by the host-metal (Ti) surface resonances (HMSR), with the dopant states dominating the gap (identified here as the states between the largest OSR and HMSR peaks either side of the Fermi level). We also note that while the Mo-doped STMO system has been used as an example,

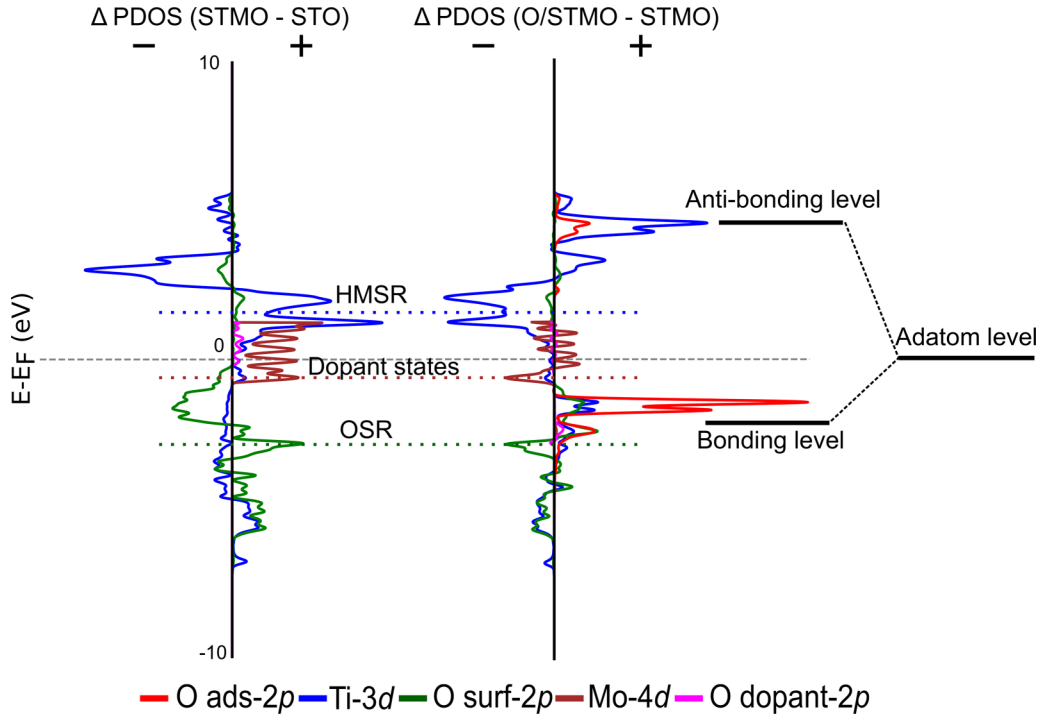


FIG. 10. Schematic illustration of the generalized concerted coupling model (GCC model). The interaction between the adatom (adsorbate) state and the oxygen surface resonance (OSR) and host-metal surface resonance (HCSR) results in the bonding and antibonding adsorbate states, captured by the quenching of the surface resonance peaks. The quenching of the dopant states in the gap shows the charge transfer from the dopant layer (Fermi level) and the newly formed bonding state. Mo-doped STMO is used as an example.

similar features are seen across all dopants and among all the host oxides considered in this study (see Figs. S33–S37 in Ref. [36] for $3d$, $4d$, and $5d$ transition metal dopants in STO, $4d$ transition metal dopants in SZO, and TiO_2 , respectively). We hypothesize that it is the states characterized by these surface resonances that are involved in the interaction with the adsorbate contributing significantly to the adsorption energy.

In order to determine the link between the surface resonances and the resultant adsorption states (by extension the adsorption energy as well), we considered the PDOS changes due to the adsorption of O on-top of the surface Ti atom of STMO as an example. The surface $\Delta\text{PDOS}(\text{STMO} - \text{STO})$ for the Mo-doped STMO is shown in Fig. 10 along with the ΔPDOS obtained due to the adsorption of O on-top the surface Ti atom, i.e., $\Delta\text{PDOS}(\text{O}/\text{STMO} - \text{STMO})$. If we consider the free adsorbate level to be characterized by a single energy level, it can interact in a concerted fashion with both the OSR's and the HCSR's, giving rise to the resultant bonding and antibonding adsorbate states. This is evident by the quenching of the surface resonances [negative peaks in $\Delta\text{PDOS}(\text{O}/\text{STMO} - \text{STMO})$ in Fig. 10] that correspond in energy to the positions of the OSR's and HCSR's in the valence and conduction band, respectively. Further, as established previously, the quenching of the dopant states in the vicinity of the Fermi level is also seen, indicative of the charge transfer from these states to the newly formed bonding level of the adsorbate. We note that the identification of the specific regions of the PDOS of the surface atoms is enabled by the perturbation of the electronic structure due to the addition of dopants to the subsurface of the oxide, aiding their

quantification in the adsorption process. The schematic illustration shown in Fig. 10 also suggests that the adsorption can now be viewed as a two-level problem involving the interaction of the adsorbate state with the OSR's and HCSR's resulting in the bonding and antibonding levels.

We can therefore write a generic expression for the adsorption energy on undoped STO or any other oxide host as

$$\begin{aligned} \Delta E_{\text{ads,STO}} &= \Delta E_{\text{hyb,STO}} + \Delta E_{\text{orthog,STO}} + \Delta E_{\text{es,STO}} \\ &= -\alpha\omega_{\text{STO}} + \Delta E_{\text{orthog,STO}} + \Delta E_{\text{es,STO}}, \quad (1) \end{aligned}$$

where $\Delta E_{\text{hyb,STO}}$ is the hybridization energy of the adsorbate on undoped STO, $\Delta E_{\text{orthog,STO}}$ is the Pauli repulsion contribution due to orbital orthogonalization, and $\Delta E_{\text{es,STO}}$ is the electrostatic contribution to the adsorption energy. The hybridization term is given by $-\alpha\omega_{\text{STO}}$ with α being related to the filling of the surface states. As identified in our electronic structure analysis above, we have established that the changes to the charge density above the surface due to dopants in the subsurface are minimal and largely set by the surface O atoms. This suggests that the decay length of the surface O- $2p$ states are roughly the same across all the doped systems and equivalent to that of the host oxide. Further the charge localization in the subsurface dopant layer [32], coupled with no changes to the filling of the surface atom states (see Fig. S31 in Ref. [36]), imply that to a first approximation we can consider the coupling strength (i.e., $V_{\text{O-}2p,\text{ads}}^2$ and $V_{\text{Ti-}3d,\text{ads}}^2$) to be equal to that of the host oxide across all the dopants, for a given adsorbate. Therefore we can now write a generic expression for the adsorption energy on the doped STMO or any other

oxide as

$$\begin{aligned}\Delta E_{\text{ads,STMO}} &= -\alpha\omega_{\text{STMO}} + \Delta E_{\text{orthog,STMO}} + \Delta E_{\text{es,STMO}} \\ &= -\alpha\omega_{\text{STMO}} + \Delta E_{\text{orthog,STO}} + \Delta E_{\text{es,STMO}},\end{aligned}\quad (2)$$

where the terms have the same meaning as above but now for the doped system. The repulsive contribution is assumed to be identical to that of the host oxide, since it is largely $\propto V_{\text{O-}2p,\text{ads}}^2$ and $V_{\text{Ti-}3d,\text{ads}}^2$, which can be approximated to be equivalent to that of the host oxide as discussed above. As established in the discussion above, the interaction of the adsorbate states with the surface resonances results in the bonding and antibonding adsorbate states, whose positions are shifted with the OSR and HMSR, which in turn is induced by the pinning of the Fermi level by the introduced dopant. Therefore, if we assume based on the evidence presented in Fig. 10 that the position of the OSR in the valence band and that of the HMSR in the conduction band are approximate indicators of the resultant bonding and antibonding states, respectively, we can now consider a perturbation expansion of the hybridization term ($-\alpha\omega_{\text{STMO}}$) to reflect the shift in the bonding and antibonding adsorbate states in the doped STMO system relative to the undoped STO host oxide. In order to obtain the perturbation parameter, we define a mean OSR (ε_{OSR}), and mean HMSR ($\varepsilon_{\text{HMSR}}$), similar to that of the d -band center [29] and ε_{CCM} [43] used for transition-metal carbides and nitrides previously. The exact formulation of ε_{OSR} and $\varepsilon_{\text{HMSR}}$ are provided in the Computational methods section. Therefore Eq. (2) can now be rewritten as

$$\Delta E_{\text{ads,STMO}} = -\alpha\omega_{\text{STO}}(1 + \varepsilon)^n + \Delta E_{\text{orthog,STO}} + \Delta E_{\text{es,STMO}},\quad (3)$$

where $\varepsilon \ll 1$ is the perturbation parameter of an n term perturbation expansion. We define ε formally as

$$\varepsilon = \left| \frac{\varepsilon_{\text{OSR}} - \varepsilon_{\text{Oads,bond,STO}}}{\varepsilon_{\text{HMSR}} - \varepsilon_{\text{Oads,antibond,STO}}} \right|,\quad (4)$$

where $\varepsilon_{\text{Oads,bond,STO}}$ and $\varepsilon_{\text{Oads,antibond,STO}}$ are the bonding and antibonding, respectively, peak positions of the adsorbate (O for example) in the host-oxide (STO for example). This essentially reflects the shift in the bonding and antibonding adsorbate states and their contributions to the adsorption energy in a consistent manner across the different doped systems. Since $\varepsilon \ll 1$ by definition, we can perform a Taylor series expansion about $\varepsilon = 0$, which gives

$$\begin{aligned}\Delta E_{\text{ads,STMO}} &= -\alpha\omega_{\text{STO}} \left(1 + n\varepsilon + \frac{1}{2}n(n-1)\varepsilon^2 + \dots \right) \\ &\quad + \Delta E_{\text{orthog,STO}} + \Delta E_{\text{es,STMO}}.\end{aligned}\quad (5)$$

Neglecting the higher order terms in the expansion, Eq. (5) can be rewritten as

$$\Delta E_{\text{ads,STMO}} = \Delta E_{\text{ads,STO}} - n\alpha\omega_{\text{STO}}\varepsilon + \Delta\Delta E_{\text{es}},\quad (6)$$

where $\Delta E_{\text{ads,STO}}$ is the adsorption energy on undoped STO (host oxide) as defined in Eq. (1), and $\Delta\Delta E_{\text{es}}$ is the difference in electrostatic energy between the doped (STMO) and host (STO) oxides. The $\Delta\Delta E_{\text{es}}$ term is formally computed using Eq. (19) in the Computational Methods section, and shown in Figs. S53–S56 in Ref. [36] for the different adsorbates. Across

the different adsorbates, its magnitude is very small compared to the other terms in Eq. (6) and can therefore be neglected.

Finally, we note that the ε can be split into two terms:

$$\varepsilon = \left| \frac{\varepsilon_{\text{OSR}}}{\varepsilon_{\text{HMSR}}} \right| * \left| \frac{1 - \frac{\varepsilon_{\text{Oads,bond,STO}}}{\varepsilon_{\text{OSR}}}}{1 - \frac{\varepsilon_{\text{Oads,antibond,STO}}}{\varepsilon_{\text{HMSR}}}} \right| = \left| \frac{\varepsilon_{\text{OSR}}}{\varepsilon_{\text{HMSR}}} \right| * \delta.\quad (7)$$

Figure S43 in Ref. [36] shows the magnitudes of the two terms in Eq. (7) for the O adsorbed on-top of the Ti surface atom for doped STMO systems. It can be seen that δ is a constant and can therefore be factored out, resulting in

$$\Delta E_{\text{ads,STMO}} \approx \Delta E_{\text{ads,STO}} - \gamma_{\text{ads,STO}} \left| \frac{\varepsilon_{\text{OSR}}}{\varepsilon_{\text{HMSR}}} \right| \quad (8)$$

or more generally,

$$\Delta E_{\text{ads,doped}} \approx \Delta E_{\text{ads,host}} - \gamma_{\text{ads,host}} \left| \frac{\varepsilon_{\text{OSR}}}{\varepsilon_{\text{HMSR}}} \right|,\quad (9)$$

where

$$\gamma_{\text{ads,host}} \approx n\alpha\delta\omega_{\text{host}} \Rightarrow \gamma_{\text{ads,host}} \propto \omega_{\text{host}} \propto V_{\text{surf,ads}}^2.\quad (10)$$

The derived Eqs. (8)–(10) suggest that (i) the adsorption energy on the doped STMO oxide varies linearly with respect to the ratio of the surface resonances (OSR to HMSR), (ii) the intercept is equal to the adsorption energy on the STO host oxide, and (iii) the slope is given by $\gamma_{\text{ads,STO}}$ ($\gamma_{\text{ads,host}}$), which is a constant for a given adsorbate and host oxide combination, but crucially depends on the coupling strength between the surface atoms of the host oxide and the adsorbate. Importantly, this shows that $|\varepsilon_{\text{OSR}}/\varepsilon_{\text{HMSR}}|$ can serve as a unique electronic structure descriptor for the electron-accepting adsorption on doped semiconducting oxides. We use this insight in the next section to correlate the adsorption energies and provide an interpretation of the adsorbate scaling relations. We also note that while STO and O have been used as the host oxide and adsorbate respectively for developing the model, other semiconducting host oxides and adsorbates may also be used equivalently.

D. Origin and interpretation of the adsorbate scaling relations

We next test the above introduced GCC model and its key finding. Figure 11 shows the correlation between the adsorption energy of OH_x ($x = 0-1$) and NH_x ($x = 0-2$) for the different doped STMO systems with respect to the identified descriptor $|\varepsilon_{\text{OSR}}/\varepsilon_{\text{HMSR}}|$. We note that as per the GCC model, the intercept in the linear fit was set to the adsorption energy of the corresponding species on undoped STO host oxide. We find a very good linear fit for all of the different adsorbates considered, validating the GCC model and the identified descriptor for the electron-accepting adsorption on doped semiconducting oxides. Interestingly, we can also see that the slopes reflect the observed scaling relations shown in Figure 2 for both OH_x and NH_x , i.e., a slope of ≈ 1 and 0.5 for O and OH, respectively, and ≈ 1 , 1, and 0.5 for N, NH, and NH_2 , respectively. Thus the origin of the scaling relations can be traced back to the common electronic structure feature that governs the adsorption of the different adsorbed species on the surface of these oxides. We can now use this result to make a generalized statement regarding the origin of the scaling

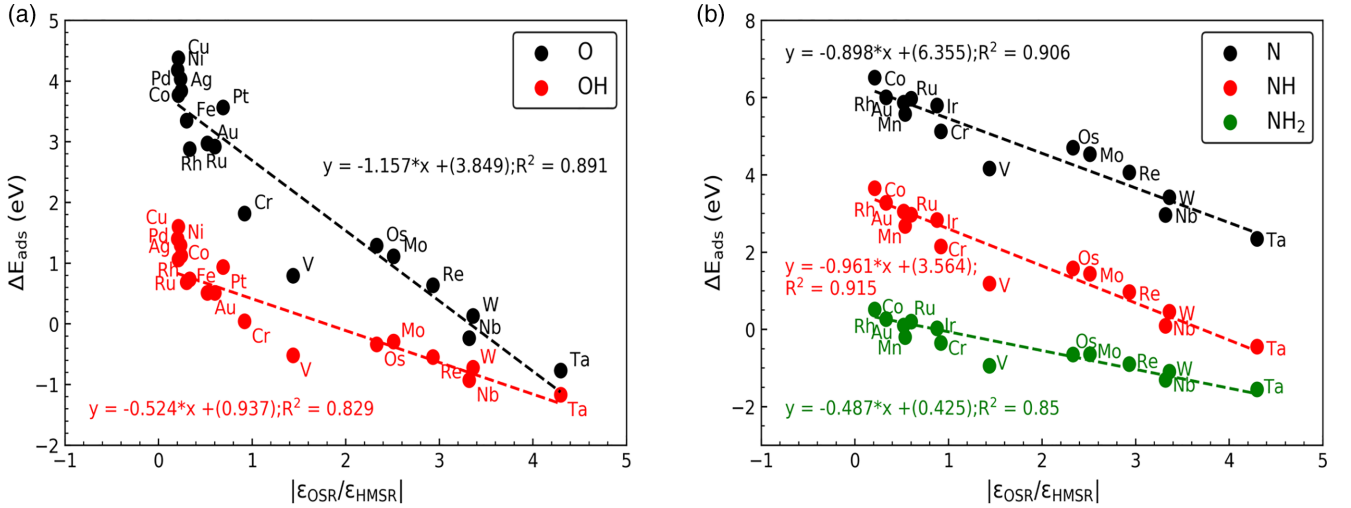


FIG. 11. Correlation between the adsorption energy of (a) OH_x ($x = 0-1$) and (b) NH_x ($x = 0-2$) adsorbed on-top of the Ti surface atom of the (001)-BO₂ surface of STMO and the identified descriptor $|\epsilon_{\text{OSR}}/\epsilon_{\text{HMSR}}|$ in the GCC model. M corresponds to $3d$, $4d$, and $5d$ transition metals doped in the subsurface of STMO. The intercept corresponds to the adsorption energy on undoped STO. The corresponding correlation plots for SZMO and TiMO₂ are shown in Figs. S50 and S51 in Ref. [36], respectively.

relations for semiconducting oxides. Finally, we note that a similar correlation is also seen for CH_x ($x = 0-3$), SH_x ($x = 0-1$), H, and OOH adsorbed on-top of the Ti surface atom on STMO; as well as OH_x ($x = 0-1$), NH_x ($x = 0-2$), and OOH adsorbed on-top of the host-metal surface atom on SZMO and TiMO₂, establishing the generality of the descriptor and model across doped semiconducting oxides (see Figs. S45-S52 in Ref. [36]).

While this is by no means a rigorous proof, and most likely one may not exist, using the key observations that lead to the development of the GCC model, we can approximate that $\Delta E_{\text{hyb,doped}}$ and $\Delta E_{\text{orthog,doped}} \propto V_{\text{O-2p,ads}}^2 \propto V_{\text{HM-d,ads}}^2$, where the coupling strength is largely set by the host oxide and remains unperturbed by the addition of dopants to the subsurface of the oxide. As established previously, this suggests that $\Delta E_{\text{orthog,doped}} \approx \Delta E_{\text{orthog,host}}$, and $\Delta E_{\text{hyb,doped}} \propto \Delta E_{\text{hyb,host}}$ but scaled by a perturbation parameter (ϵ) for a given dopant-host combination, which explains the observed slopes in the correlation, since $\gamma_{\text{ads,host}} \propto \Delta E_{\text{hyb,host}}$ [see Eq. (1)]. Therefore, for the systems considered here, we suggest that the scaling slope $\gamma(x) \propto V_{\text{O-2p,ads}}^2$ and $V_{\text{HM-d,ads}}^2$, set primarily by the host oxide for a given adsorbate. However, we note that the relative coupling strengths is a function of the distances between the adsorbate and the surface atoms ($V^2[\mathbf{r}]$). Since the oxide surface is composed of two disparate adsorption sites in the form of the host metal surface atoms and the oxygen surface atoms, changes in the relative position of an adsorbate relative to one site has an inverse effect with respect to the other. Ideally, the optimal bond lengths are set by where the adsorbate gets the optimal charge density from the surface, but on an inhomogeneous surface composed of metal and oxygen atoms, there is a difference in charge density across the surface as shown in Fig. S32 in Ref. [36]. This we note has a profound impact on the optimal bond length when comparing adsorbates of different electronegativities.

While highly electronegative adsorbates, e.g., O and S, adsorb optimally on the surface host-metal site resulting in

an optimal coupling with the host metal, less electronegative adsorbates, e.g., N, C (and H) may move closer to the surface oxygen resulting in an electropositive adsorption in the extreme case (as seen for H which prefers to adsorb on-top of the O surface atom over the host metal). The higher bond lengths relative to the surface Ti atom seen for N and C (see the electronic structure analysis discussion above) is essentially a consequence of this effect, where they now end up being closer to the surface oxygen site compared to O. This results in a weaker coupling with the surface host metal which consequently results in a smaller split of the bonding and antibonding adsorbate states ultimately resulting in the bonding states becoming partially unfilled as they cross the Fermi level. In addition, this also results in optimal bond lengths that are almost identical to more electron rich adsorbates as they start getting saturated with the addition of H, as seen with N and NH for example with average bond lengths of ≈ 1.8 and 1.75 Å, respectively (versus O and OH with ≈ 1.65 and 1.82 Å, respectively). This essentially results in similar coupling strengths for N and NH (versus stronger coupling for O versus OH as would be expected), also resulting in a scaling slope of ≈ 1 (versus a scaling slope of ≈ 0.5 for O and OH), since $\gamma(x) \propto V_{\text{O-2p,ads}}^2$ (and $V_{\text{HM-d,ads}}^2$). This establishes the origin of the anomalous scaling relations observed in these systems. In the final section, we will explore the extension of the model to the electron-donating adsorption, exemplified by the adsorption of H on the surface O atom.

E. Adsorption on-top of the surface oxygen atom sites

In order to understand the electron-donating adsorption as observed for H adsorbed on-top of the O surface atom, we again performed a set of *in silico* experiments to decipher the link between the electronic structure and the adsorption energy. Here we build from the set of calculations performed by moving H adsorbate across the surface from on-top of the

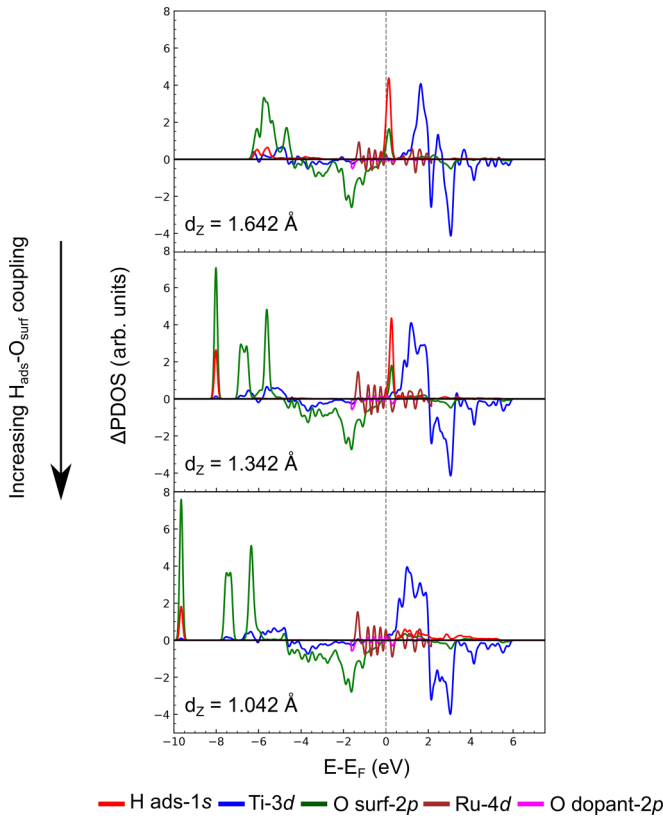


FIG. 12. The changes in the Δ PDOS, with increasing coupling strength (top to bottom) between the H adsorbate and surface O atom on Ru-doped STMO. The Δ PDOS of the surface atoms, dopant layer atoms and the adsorbate are shown.

Ti to on-top of the O atom (see Fig. 7). Once H has been moved on-top of O we then pushed it closer towards the surface. Specifically, we calculated the changes of the Δ PDOS, with increasing coupling between the H adsorbate and surface O, until we approached the distance above the surface O atom that corresponds to that of the geometry optimized bond length of H adsorbed on O (≈ 1 Å). We illustrate the changes in interaction by considering the Ru-doped STMO system as an example (Fig. 12), however, the same behavior is observed for other doped STMO systems (see Figs. S28 and S29 in Ref. [36]).

Going from top to bottom in Fig. 12, decreasing the distance (along the surface normal) between the H adsorbate and the surface O results in increasing the coupling strength between the two (see top to bottom subfigures in Fig. 12). The top subfigure in Fig. 12 corresponds to that of H placed on-top of the surface O at a distance 1.642 Å away [note this is equivalent to the bottom subfigure in Fig. 7(b)] showing the formation of a low lying adsorbate bonding state, with the adsorbate antibonding state just above the Fermi level due to the poor splitting caused by a lower coupling strength. Pushing H towards the surface O (1.342 Å distance above the O), increases the split between the bonding and antibonding adsorbate states, with the bonding state pushed to even lower energies (≈ -8 eV), and the antibonding state pushed slightly further above the Fermi level. Further, the

predominantly strong H-1s character of the antibonding state starts to diminish and is accompanied by the sharp O-2p character of the bonding state, as well as appearance of positive peaks associated with the dopant states in the vicinity of the Fermi level suggesting a charge transfer from the H-adsorbate to the dopant layer. This becomes even more prominent at a H binding position 1.042 Å above the O surface atom (bottom subfigure in Fig. 12) as the bonding state is pushed to ≈ -10 eV below the Fermi level, with the antibonding state becoming diffuse and predominantly of Ti-3d character, suggesting a concerted coupling effect. This charge transfer is also reflected by the calculated Bader charges, where the H adsorbate donates more charge to the oxide as it is pushed towards the surface (for Ru-doped STMO; the charge on H goes from: +0.13 e to +0.32 e to +0.53 e corresponding to the three probed distances above the surfaces in Fig. 12), and the surface atoms and the dopant layer atoms gaining charge. While the charge on the H adsorbate is almost constant across the dopants when placed at the optimized bond lengths, its change as H is pushed toward the surface is very different. For example, in the case of Nb-doped STMO the charge on H goes from -0.01 e to +0.22 e to +0.55 e corresponding to the same distances above the surface as for the Ru-doped STMO. The adsorption energy trends also reflect these changes in the charge transfer, with the “reverse check-mark” shape maintained (Nb and Mo highest, and Ag lowest among the 4d transition metal dopants) with increasing coupling between H and O, and the adsorption becoming stronger as the coupling strength increases.

Based on these observations, we hypothesize that a crucial piece of the electronic structure that contributes to the observed adsorption energy trend is the charge transfer from the H-1s antibonding states as they start to get unfilled to the states at and in the vicinity of the Fermi level which is dominated by the dopant states, and the surface atom states below the Fermi level. We find that the position of the H-1s antibonding states seem to be correlated to the positions of the host-metal surface resonances (HMSR) in the conduction band (see Figs. 9 and 12). This naturally suggests that the adsorption energy should be inversely related to the position of the oxygen surface resonances (OSR) in the valence band, since the shift in the surface resonances is linear across the different doped systems (from left to right along a period). This also agrees with the observations made with the Δ PDOS of the geometry optimized system, see Fig. S8 in Ref. [36] where the filled bonding peaks are much lower in energy for Nb-doped STMO compared to that of Ag-doped STMO (and antibonding states are unfilled), yet with the opposite trend in the adsorption energy (Nb highest and Ag lowest) [32]. Extending this idea within the context of the GCC model, we hypothesize that the inverse of the descriptor for the electron-accepting adsorption, i.e., $|\epsilon_{\text{HMSR}}/\epsilon_{\text{OSR}}|$ should be a suitable descriptor for the electron-donating adsorption. Figure 13 shows the adsorption energy plotted versus the descriptor $|\epsilon_{\text{HMSR}}/\epsilon_{\text{OSR}}|$ for the case where the surface atoms were constrained (to avoid any surface geometry effects which were pronounced for the adsorption of H on-top of the surface O atom); with the intercept fixed to that of the adsorption of H on-top of the surface O atom of undoped STO. We obtain a very good correlation between the adsorption energy and the identified descriptor

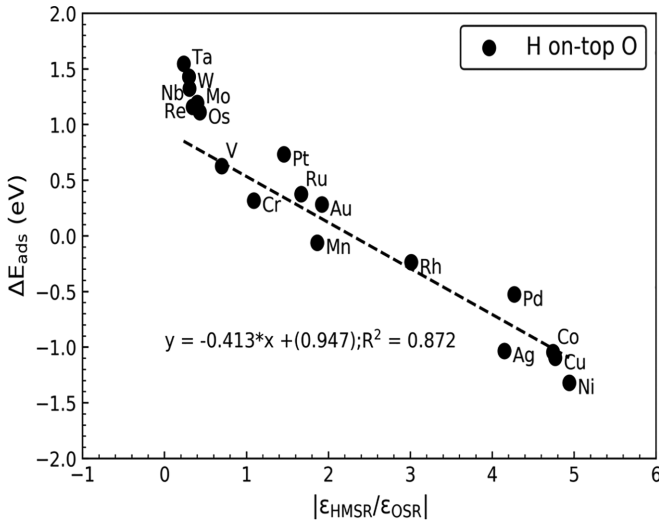


FIG. 13. Correlation between the DFT calculated adsorption energy of H adsorbed on-top of the O atom of the (001)-BO₂ surface (constrained) of STMO and the inverse of the identified descriptor in GCC model. M corresponds to 3d, 4d, and 5d transition metals doped in the subsurface of STO. The intercept corresponds to the adsorption energy on undoped STO.

suggesting that the general concepts of the GCC model are applicable to the electron-donating adsorption as well. The analysis for the adsorption of H on-top of the surface O atom is not too dissimilar to the antibonding electron transfer concept suggested for the adsorption of hydrogen on MoS₂ surfaces recently, where a similar behavior is observed [45]. Therefore we have established that the principles of the GCC model are applicable across subsurface doped semiconducting oxides for different adsorbates interacting with the surface atoms.

III. CONCLUSION

We developed a physics based adsorption model that captures the interaction between atoms and molecules with the surface of semiconducting oxides with dopants added to the subsurface. The addition of dopants served as a controlled tuning parameter to perturb the electronic structure of the surface states of the host oxide, resulting in unique surface resonances of both metallic and oxygen character whose interaction with the adsorbate was found to play a critical role in the adsorption. This coupled with a series of precise *in silico* experiments enabled the identification of the concerted coupling nature of the adsorption on these oxide surfaces, leading to the development of the generalized concerted coupling model (GCC model). The model allowed us to identify an electronic structure descriptor based on the surface specific states that was found to correlate very well with the DFT calculated adsorption energies. Interestingly, we also found deviations from the adsorbate scaling relations for certain set of adsorbates, e.g., NH_x ($x = 0-2$) and CH_x ($x = 0-3$) as compared to the ones previously found for adsorption on metals and transition metal compounds. The origin of the adsorbate scaling relation is explained within the context of the developed GCC model.

We emphasize that the development of the GCC model and the electronic structure descriptor was made possible due to the identification of the relevant states in the PDOS of the surface atoms that participate in the interaction with the adsorbate, which remains the major impediment towards the further generalization of our understanding of adsorption on surfaces across different material groups. We think that the recipes presented here can be used in the analysis of the adsorption process on other transition metal oxides, and more generally transition metal compounds where a physics based predictive understanding is still lacking. It is also our hope that with the ever increasing availability of large datasets across different materials, it may soon be possible to further generalize the approach presented in this study.

IV. COMPUTATIONAL METHODS

A. Density functional theory (DFT)

First-principles DFT calculations were performed using the QUANTUM ESPRESSO software package [46,47], and setup using the atomic simulation environment (ASE) [48]. Kohnsham wave functions were expanded using a plane-wave basis set with a kinetic energy cutoff of 500 eV. Spin polarization was neglected since we are interested in generalized trends in this study. Exchange and correlation were described within the generalized gradient approximation (GGA) using the Perdew-Burke-Ernzerhof (PBE) functional [49]. Ultrasoft pseudopotentials were used to describe the core electrons [50]. While corrections such as the Hubbard- U parameter [51] may further improve the description of the electronic structure, we have shown in our previous study that they are not necessary to gain generalized trends across the doped semiconducting oxides considered [32]. Further tests of the Hubbard- U parameter on the electronic structure, and in particular the identified descriptor in the GCC model was performed for the rutile TiO₂(110) surface doped with 4d transition metals in the subsurface. An effective U value of 2.0 eV was applied to the Ti atoms as validated in prior studies [44]. The corresponding Δ PDOS of the surface atoms with the application of the Hubbard- U corrections and the computed descriptor values are shown in Fig. S38 and Table S2 in Ref. [36], respectively. It can be seen that the addition of the Hubbard- U parameter only has a very negligible influence on the identified descriptor.

The (001)-BO₂ termination of the perovskite oxides (STO and SZO), and the (110) surface of the rutile oxide TiO₂ were considered for computing the adsorption energies of all the adsorbates considered in this study. A $2 \times 2 \times 4$ supercell was used to represent all the surfaces with the bottom two layers fixed to their bulk-lattice positions. Additional tests involving the influence of the number of layers in the slab model on the adsorption energy was also performed for the undoped rutile TiO₂(110) surface and is provided in Table S1 in Ref. [36]. It can be seen that the change in adsorption energy of O is only ≈ 0.05 eV between four- and five-layer slab models. We used the geometry optimized surfaces and lattice constants reported in our previous study [32] to compute the adsorption energies of the different adsorbates. Periodic boundary conditions were applied in all directions with a vacuum

spacing of at least 14 Å separating the surfaces in the z direction to prevent interaction between periodic images. Dipole corrections were also applied along the surface normal to account for the surface asymmetry. The Brillouin zone was sampled using a $(4 \times 4 \times 1)$ Monkhorst-Pack grid [52] for the geometry optimization calculations, with a finer grid used for the electronic structure calculations. The relaxed geometries were considered optimized when the maximum force on all atoms in the system was less than 0.03 eV/Å. Bader charge analysis was performed using a grid-based decomposition scheme of the electron density [53].

Adsorption energy was computed as

$$\Delta E_{\text{ads}} = E_{\text{surf,ads}} - E_{\text{surf}} - E_{\text{ads}}, \quad (11)$$

where ΔE_{ads} is the adsorption energy, $E_{\text{surf,ads}}$ is the energy of the geometry optimized surface with the adsorbate, E_{surf} is the energy of the geometry optimized pristine surface and E_{ads} is the energy of the adsorbate in its reference state. We used the same reference for the OH_x ($x = 0-1$), OOH and H adsorbates as in our previous study [32]. NH_x ($x = 0-2$) species were referenced to N_2 and H_2 in the gas phase. CH_x ($x = 0-3$) species were referenced to CH_4 and H_2 in the gas phase. SH_x ($x = 0-1$) species were referenced to H_2S and H_2 in the gas phase.

Specifically, the following equations were used to compute the adsorption energies of the NH_x ($x = 0-2$), CH_x ($x = 0-3$), and SH_x ($x = 0-1$) species:

$$\Delta E_{\text{NH}_x} = E_{\text{surf,NH}_x} - E_{\text{surf}} - \left[\frac{1}{2} E_{\text{N}_2} + \frac{x}{2} E_{\text{H}_2} \right], \quad (12)$$

$$\Delta E_{\text{CH}_x} = E_{\text{surf,CH}_x} - E_{\text{surf}} - \left[E_{\text{CH}_4} - \frac{4-x}{2} E_{\text{H}_2} \right], \quad (13)$$

$$\Delta E_{\text{SH}_x} = E_{\text{surf,SH}_x} - E_{\text{surf}} - \left[E_{\text{H}_2\text{S}} - \frac{2-x}{2} E_{\text{H}_2} \right]. \quad (14)$$

Additional tests involving gas-phase radicals as the reference state were also performed for the NH_x ($x = 0-2$) adsorbates. The adsorption energy scaling relations for adsorption on-top the Ti atom of the (001)- BO_2 surface of STMO and the correlation of the adsorption energy with the descriptor identified in the GCC model using these reference states are shown in Figs. S2 and S49, respectively, in Ref. [36]. It can be seen that the scaling slopes and the correlations are identical to those shown in Figs. 2(b) and 11(b), indicating that the choice of reference state has no influence on the GCC model.

B. Electronic structure analysis and adsorption models

The atom projected electronic density of states (PDOS) for the various different systems were obtained from DFT. In general, the n th moment of the distribution was computed as

$$m_n = \frac{\int_{-\infty}^{\infty} \varepsilon^n \rho(\varepsilon) d\varepsilon}{\int_{-\infty}^{\infty} \rho(\varepsilon) d\varepsilon}, \quad (15)$$

where the first moment gives the band center and the zeroth moment integrated up to the Fermi level gives the filling. In all of the analysis in this study, the electronic density of states are calculated relative to the Fermi level of the system which is set as 0 on the relative energy scale.

The first moment of the oxygen (OSR) and host-metal states (HMSR) characterized by their respective surface resonances identified from the Δ PDOS are defined as

$$\varepsilon_{\text{OSR}} = \frac{\int_{\varepsilon_{\text{OVB}}}^{\varepsilon_{\text{gap}}} \varepsilon \rho_{\text{O},2p}(\varepsilon) d\varepsilon}{\int_{\varepsilon_{\text{OVB}}}^{\varepsilon_{\text{gap}}} \rho_{\text{O},2p}(\varepsilon) d\varepsilon} \quad (16)$$

and

$$\varepsilon_{\text{HMSR}} = \frac{\int_{\varepsilon_{\text{gap}}}^{\varepsilon_{\text{HMCB}}} \varepsilon \rho_{\text{HM},d}(\varepsilon) d\varepsilon}{\int_{\varepsilon_{\text{gap}}}^{\varepsilon_{\text{HMCB}}} \rho_{\text{HM},d}(\varepsilon) d\varepsilon}, \quad (17)$$

where ε_{OVB} is the first moment of the positive surface resonance of the O-2p states in the valence band, $\varepsilon_{\text{HMCB}}$ is the first moment of the positive surface resonance of the HM- d states in the conduction band, and ε_{gap} is the first moment of the gap states composed of both the dopant metal and the lattice oxygen in the dopant layer in the subsurface of the host oxide. The gap states are identified by the positive surface states composed of the dopant d states and oxygen (dopant-layer) p states between the highest surface O-2p resonance in the valence band and the highest surface HM- d resonance in the conduction band.

In order to develop the generalized concerted coupling model, we draw inspiration from existing adsorption models; namely the Newns-Anderson [40,41], d -band [29], and the concerted coupling models [43]. Specifically, the identification and definition of the first moment of the surface resonances follow directly from the concerted coupling model developed for transition metal carbides and nitrides [42,43,54]. To establish the concerted coupling nature of the interaction of adsorbates with the doped semiconducting oxides considered in this study, we utilize the Newns-Anderson model by assuming that the adsorbate interacts independently with both the surface HM- d and O-2p states, characterized by different coupling matrix elements. Thus the resultant hybridization energy is given by

$$\Delta E_{\text{hyb}} = \frac{2}{\pi} \left[\int_{-\infty}^0 \text{Arctan} \left(\frac{\Delta_d(\varepsilon)}{\varepsilon - \varepsilon_a - \Lambda_d(\varepsilon)} \right) d\varepsilon + \int_{-\infty}^0 \text{Arctan} \left(\frac{\Delta_p(\varepsilon)}{\varepsilon - \varepsilon_a - \Lambda_p(\varepsilon)} \right) d\varepsilon \right] - n_a \varepsilon_a, \quad (18)$$

where ε_a is the adsorbate state which is treated as a constant in our study, for a given adsorbate. $\Delta_d(\varepsilon)$ and $\Delta_p(\varepsilon)$ are the chemisorption functions which describe the interaction between the adsorbate and the surface HM- d and O-2p states, respectively. For a qualitative discussion of the adsorption energy trends in this study, the average coupling matrix element may be used in the chemisorption function, as used previously for metals [55]. Therefore the chemisorption functions are defined as $\Delta_d(\varepsilon) = \pi V_{\text{HM,ads}}^2 \rho_{\text{HM},d}(\varepsilon)$, and $\Delta_p(\varepsilon) = \pi V_{\text{O,ads}}^2 \rho_{\text{O},2p}(\varepsilon)$, where $V_{\text{HM,ads}}^2$ and $V_{\text{O,ads}}^2$ are the average coupling strength between the adsorbate and the surface HM- d and O-2p states, respectively. $\rho_{\text{HM},d}(\varepsilon)$ and $\rho_{\text{O},2p}(\varepsilon)$ are the projected density of states of the surface HM- d and O-2p atoms in the pristine surface unperturbed by the adsorbate. $\Lambda_d(\varepsilon)$ and $\Lambda_p(\varepsilon)$ are obtained from the Hilbert transform

of the corresponding chemisorption functions, $\Delta_d(\varepsilon)$ and $\Delta_p(\varepsilon)$.

Electrostatic contributions to the adsorption energy were considered in the model relative to that of the host oxide without the addition of dopants. This relative electrostatic energy is given by

$$\Delta E_{\text{es}} = 1/2 \int \Delta n_{\text{ads,host}}(z) \Delta V_{\text{dop}}(z) dx dy dz, \quad (19)$$

where $\Delta n_{\text{ads,host}}(z)$ is the $x - y$ averaged charge density difference induced by the adsorbate on the host oxide (STO, SZO or TiO_2); i.e., $\Delta n_{\text{ads,host}}(z) = n_{\text{ads,host}} - n_{\text{host}} - n_{\text{ads}}$, and $\Delta V_{\text{dop}}(z)$ is the $x - y$ averaged change in the electrostatic potential due to the addition of dopants to the host oxide. The integration should be performed over the volume corresponding to the region of the adsorbate. In this study, we instead

approximate this to be over the entire cell, as used previously on metal surfaces [56].

ACKNOWLEDGMENTS

A.V. acknowledges the Canadian institute for Advanced research (CIFAR) for support through the Accelerated Decarbonization Program. The authors acknowledge the use of the computer time allocation at the National Energy Research Scientific Computing Center (NERSC), a DOE Office of Science User Facility supported by the Office of Science of the US Department of Energy under Contract No. DE-AC02-05CH11231 and the computing resources (Stampede2 at TACC) provided by the Extreme Science and Engineering Discovery Environment (XSEDE) supported through the National Science Foundation (NSF) under Award No. DMR180108.

-
- [1] A. Selloni, Titania and its outstanding properties: Insights from first principles calculations, in *Handbook of Materials Modeling: Applications: Current and Emerging Materials*, edited by W. Andreoni and S. Yip (Springer, Cham, 2020), pp. 29–51.
- [2] R. Rousseau, V. A. Glezakou, and A. Selloni, Theoretical insights into the surface physics and chemistry of redox-active oxides, *Nat. Rev. Mater.* **5**, 460 (2020).
- [3] W. T. Hong, M. Risch, K. A. Stoerzinger, A. Grimaud, J. Suntivich, and Y. Shao-Horn, Toward the rational design of non-precious transition metal oxides for oxygen electrocatalysis, *Energy Environ. Sci.* **8**, 1404 (2015).
- [4] Z. W. Seh, J. Kibsgaard, C. F. Dickens, I. Chorkendorff, J. K. Nørskov, and T. F. Jaramillo, Combining theory and experiment in electrocatalysis: Insights into materials design, *Science* **355**, eaad4998 (2017).
- [5] G. S. Parkinson and U. Diebold, Adsorption on metal oxide surfaces, in *Surface and Interface Science*, edited by K. Wandelt (John Wiley & Sons, 2016), Chap. 44, pp. 793–817.
- [6] C. T. Campbell and J. Sauer, Introduction: Surface chemistry of oxides, *Chem. Rev.* **113**, 3859 (2013).
- [7] G. Pacchioni, Electronic interactions and charge transfers of metal atoms and clusters on oxide surfaces, *Phys. Chem. Chem. Phys.* **15**, 1737 (2013).
- [8] F. Calle-Vallejo, N. G. Inoglu, H.-Y. Su, J. I. Martínez, I. C. Man, M. T. M. Koper, J. R. Kitchin, and J. Rossmeisl, Number of outer electrons as descriptor for adsorption processes on transition metals and their oxides, *Chem. Sci.* **4**, 1245 (2013).
- [9] J. Suntivich, K. J. May, H. A. Gasteiger, J. B. Goodenough, and Y. Shao-Horn, A perovskite oxide optimized for oxygen evolution catalysis from molecular orbital principles, *Science* **334**, 1383 (2011).
- [10] A. Grimaud, K. J. May, C. E. Carlton, Y. L. Lee, M. Risch, W. T. Hong, J. Zhou, and Y. Shao-Horn, Double perovskites as a family of highly active catalysts for oxygen evolution in alkaline solution, *Nat. Commun.* **4**, 2439 (2013).
- [11] Y.-L. Lee, M. J. Gadre, Y. Shao-Horn, and D. Morgan, Ab initio GGA+U study of oxygen evolution and oxygen reduction electrocatalysis on the (001) surfaces of lanthanum transition metal perovskites LaBO_3 ($B = \text{Cr, Mn, Fe, Co}$ and Ni), *Phys. Chem. Chem. Phys.* **17**, 21643 (2015).
- [12] J. H. Montoya, A. D. Doyle, J. K. Nørskov, and A. Vojvodic, Trends in adsorption of electrocatalytic water splitting intermediates on cubic ABO_3 oxides, *Phys. Chem. Chem. Phys.* **20**, 3813 (2018).
- [13] R. Jacobs, J. Hwang, Y. Shao-Horn, and D. Morgan, Assessing correlations of perovskite catalytic performance with electronic structure descriptors, *Chem. Mater.* **31**, 785 (2019).
- [14] C. F. Dickens, J. H. Montoya, A. R. Kulkarni, M. Bajdich, and J. K. Nørskov, An electronic structure descriptor for oxygen reactivity at metal and metal-oxide surfaces, *Surf. Sci.* **681**, 122 (2019).
- [15] W. T. Hong, K. A. Stoerzinger, Y.-L. Lee, L. Giordano, A. Grimaud, A. M. Johnson, J. Hwang, E. J. Crumlin, W. Yang, and Y. Shao-Horn, Charge-transfer-energy-dependent oxygen evolution reaction mechanisms for perovskite oxides, *Energy Environ. Sci.* **10**, 2190 (2017).
- [16] X. Huang, J. Wang, H. B. Tao, H. Tian, and H. Xu, An essential descriptor for the oxygen evolution reaction on reducible metal oxide surfaces, *Chem. Sci.* **10**, 3340 (2019).
- [17] D. Wu, C. Dong, H. Zhan, and X.-W. Du, Bond-energy-integrated descriptor for oxygen electrocatalysis of transition metal oxides, *J. Phys. Chem. Lett.* **9**, 3387 (2018).
- [18] B. M. Comer, J. Li, F. Abild-Pedersen, M. Bajdich, and K. T. Winther, Unraveling electronic trends in O^* and OH^* surface adsorption in the MO_2 transition-metal oxide series, *J. Phys. Chem. C* **126**, 7903 (2022).
- [19] W. T. Hong, R. E. Welsch, and Y. Shao-Horn, Descriptors of oxygen-evolution activity for oxides: A statistical evaluation, *J. Phys. Chem. C* **120**, 78 (2016).
- [20] W. Xu, M. Andersen, and K. Reuter, Data-driven descriptor engineering and refined scaling relations for predicting transition metal oxide reactivity, *ACS Catal.* **11**, 734 (2021).

- [21] Z. Li, L. E. K. Achenie, and H. Xin, An adaptive machine learning strategy for accelerating discovery of perovskite electrocatalysts, *ACS Catal.* **10**, 4377 (2020).
- [22] P. S. Bagus and F. Illas, Decomposition of the chemisorption bond by constrained variations: Order of the variations and construction of the variational spaces, *J. Chem. Phys.* **96**, 8962 (1992).
- [23] G. Pacchioni, C. Sousa, F. Illas, F. Parmigiani, and P. S. Bagus, Measures of ionicity of alkaline-earth oxides from the analysis of ab initio cluster wave functions, *Phys. Rev. B* **48**, 11573 (1993).
- [24] G. Pacchioni, A. Clotet, and J. M. Ricart, A theoretical study of the adsorption and reaction of SO₂ at surface and step sites of the MgO(100) surface, *Surf. Sci.* **315**, 337 (1994).
- [25] G. Pacchioni, J. M. Ricart, and F. Illas, Ab initio cluster model calculations on the chemisorption of CO₂ and SO₂ probe molecules on MgO and CaO (100) surfaces. A theoretical measure of oxide basicity, *J. Am. Chem. Soc.* **116**, 10152 (1994).
- [26] G. Pacchioni, A. M. Ferrari, and P. S. Bagus, Cluster and band structure ab initio calculations on the adsorption of CO on acid sites of the TiO₂(110) surface, *Surf. Sci.* **350**, 159 (1996).
- [27] J. Casanovas, J. Rubio, and F. Illas, Origin of magnetic coupling in La₂CuO₄, *Phys. Rev. B* **53**, 945 (1996).
- [28] N. Cruz Hernández, C. M. Zicovich-Wilson, and J. Fdez. Sanz, The constrained space orbital variation analysis for periodic ab initio calculations, *J. Chem. Phys.* **124**, 194105 (2006).
- [29] B. Hammer and J. K. Nørskov, Electronic factors determining the reactivity of metal surfaces, *Surf. Sci.* **343**, 211 (1995).
- [30] W. S. Choi, S. Lee, V. R. Cooper, and H. N. Lee, Fractionally δ -doped oxide superlattices for higher carrier mobilities, *Nano Lett.* **12**, 4590 (2012).
- [31] A. R. Akbashev, L. Zhang, J. T. Mefford, J. Park, B. Butz, H. Luftman, W. C. Chueh, and A. Vojvodic, Activation of ultrathin SrTiO₃ with subsurface SrRuO₃ for the oxygen evolution reaction, *Energy Environ. Sci.* **11**, 1762 (2018).
- [32] L. Zhang, A. S. Raman, and A. Vojvodic, Reviving inert oxides for electrochemical water splitting by subsurface engineering, *Chem. Mater.* **32**, 5569 (2020).
- [33] E. M. Fernández, P. G. Moses, A. Toftelund, H. A. Hansen, J. Martínez, F. Abild-Pedersen, J. Kleis, B. Hinnemann, J. Rossmeisl, T. Bligaard, and J. K. Nørskov, Scaling relationships for adsorption energies on transition metal oxide, sulfide, and nitride surfaces, *Angew. Chem. Int. Ed.* **47**, 4683 (2008).
- [34] I. C. Man, H. Y. Su, F. Calle-Vallejo, H. A. Hansen, J. I. Martínez, N. G. Inoglu, J. Kitchin, T. F. Jaramillo, J. K. Nørskov, and J. Rossmeisl, Universality in oxygen evolution electrocatalysis on oxide surfaces, *ChemCatChem* **3**, 1159 (2011).
- [35] F. Abild-Pedersen, J. Greeley, F. Studt, J. Rossmeisl, T. R. Munter, P. G. Moses, E. Skúlason, T. Bligaard, and J. K. Nørskov, Scaling properties of adsorption energies for hydrogen-containing molecules on transition-metal surfaces, *Phys. Rev. Lett.* **99**, 016105 (2007).
- [36] See Supplemental Material at <http://link.aps.org/supplemental/10.1103/PhysRevB.109.195416> for computational results including: the scaling relations involving different adsorbates; changes to the projected density of states (PDOS) due to adsorption, the different surface sites, adsorption geometry, and dopants; charge density difference; correlation with the identified descriptor; electrostatic contributions; and Bader charges.
- [37] J. K. Nørskov and N. D. Lang, Effective-medium theory of chemical binding: Application to chemisorption, *Phys. Rev. B* **21**, 2131 (1980).
- [38] H. Xin and S. Linic, Communications: Exceptions to the d-band model of chemisorption on metal surfaces: The dominant role of repulsion between adsorbate states and metal d-states, *J. Chem. Phys.* **132**, 221101 (2010).
- [39] S. Y. Davydov and S. V. Troshin, Adsorption on metals and semiconductors: Anderson-Newns and Haldane-Anderson models, *Phys. Solid State* **49**, 1583 (2007).
- [40] D. M. Newns, Self-consistent model of hydrogen chemisorption, *Phys. Rev.* **178**, 1123 (1969).
- [41] T. B. Grimley, Overlap effects in the theory of adsorption using Anderson's hamiltonian, *J. Phys. C: Solid State Phys.* **3**, 1934 (1970).
- [42] C. Ruberto, A. Vojvodic, and B. I. Lundqvist, Nature of chemisorption on titanium carbide and nitride, *Surf. Sci.* **600**, 1612 (2006).
- [43] A. Vojvodic, A. Hellman, C. Ruberto, and B. I. Lundqvist, From electronic structure to catalytic activity: A single descriptor for adsorption and reactivity on transition-metal carbides, *Phys. Rev. Lett.* **103**, 146103 (2009).
- [44] M. García-Mota, A. Vojvodic, F. Abild-Pedersen, and J. K. Nørskov, Electronic origin of the surface reactivity of transition-metal-doped TiO₂ (110), *J. Phys. Chem. C* **117**, 460 (2013).
- [45] L. Yu, Q. Yan, and A. Ruzsinszky, Key role of antibonding electron transfer in bonding on solid surfaces, *Phys. Rev. Mater.* **3**, 092801(R) (2019).
- [46] P. Giannozzi, S. Baroni, N. Bonini, M. Calandra, R. Car, C. Cavazzoni, D. Ceresoli, G. L. Chiarotti, M. Cococcioni, I. Dabo, A. Dal Corso, S. de Gironcoli, S. Fabris, G. Fratesi, R. Gebauer, U. Gerstmann, C. Gougoussis, A. Kokalj, M. Lazzeri, L. Martin-Samos *et al.*, QUANTUM ESPRESSO: a modular and open-source software project for quantum simulations of materials, *J. Phys.: Condens. Matter* **21**, 395502 (2009).
- [47] P. Giannozzi, O. Andreussi, T. Brumme, O. Bunau, M. Buongiorno Nardelli, M. Calandra, R. Car, C. Cavazzoni, D. Ceresoli, M. Cococcioni, N. Colonna, I. Carnimeo, A. Dal Corso, S. de Gironcoli, P. Delugas, R. A. DiStasio, Jr., A. Ferretti, A. Floris, G. Fratesi, G. Fugallo *et al.*, Advanced capabilities for materials modelling with Quantum ESPRESSO, *J. Phys.: Condens. Matter* **29**, 465901 (2017).
- [48] A. Hjorth Larsen, J. Jørgen Mortensen, J. Blomqvist, I. E. Castelli, R. Christensen, M. Dułak, J. Friis, M. N. Groves, B. Hammer, C. Hargus, E. D. Hermes, P. C. Jennings, P. Bjerre Jensen, J. Kermode, J. R. Kitchin, E. Leonhard Kolsbjerg, J. Kubal, K. Kaasbjerg, S. Lysgaard, J. Bergmann Maronsson *et al.*, The atomic simulation environment—a Python library for working with atoms, *J. Phys.: Condens. Matter* **29**, 273002 (2017).
- [49] J. P. Perdew, K. Burke, and M. Ernzerhof, Generalized gradient approximation made simple, *Phys. Rev. Lett.* **77**, 3865 (1996).

- [50] D. Vanderbilt, Soft self-consistent pseudopotentials in a generalized eigenvalue formalism, *Phys. Rev. B* **41**, 7892 (1990).
- [51] V. I. Anisimov, J. Zaanen, and O. K. Andersen, Band theory and mott insulators: Hubbard U instead of stoner I, *Phys. Rev. B* **44**, 943 (1991).
- [52] H. J. Monkhorst and J. D. Pack, Special points for Brillouin-zone integrations, *Phys. Rev. B* **13**, 5188 (1976).
- [53] G. Henkelman, A. Arnaldsson, and H. Jónsson, A fast and robust algorithm for Bader decomposition of charge density, *Comput. Mater. Sci.* **36**, 354 (2006).
- [54] C. Ruberto and B. I. Lundqvist, Nature of adsorption on TiC(111) investigated with density-functional calculations, *Phys. Rev. B* **75**, 235438 (2007).
- [55] A. Vojvodic, J. K. Nørskov, and F. Abild-Pedersen, Electronic structure effects in transition metal surface chemistry, *Top. Catal.* **57**, 25 (2014).
- [56] H. Xin and S. Linic, Analyzing relationships between surface perturbations and local chemical reactivity of metal sites: Alkali promotion of O₂ dissociation on Ag(111), *J. Chem. Phys.* **144**, 234704 (2016).